Techno-Economic Analysis of a Heat Sink for Micro Chip Cooling

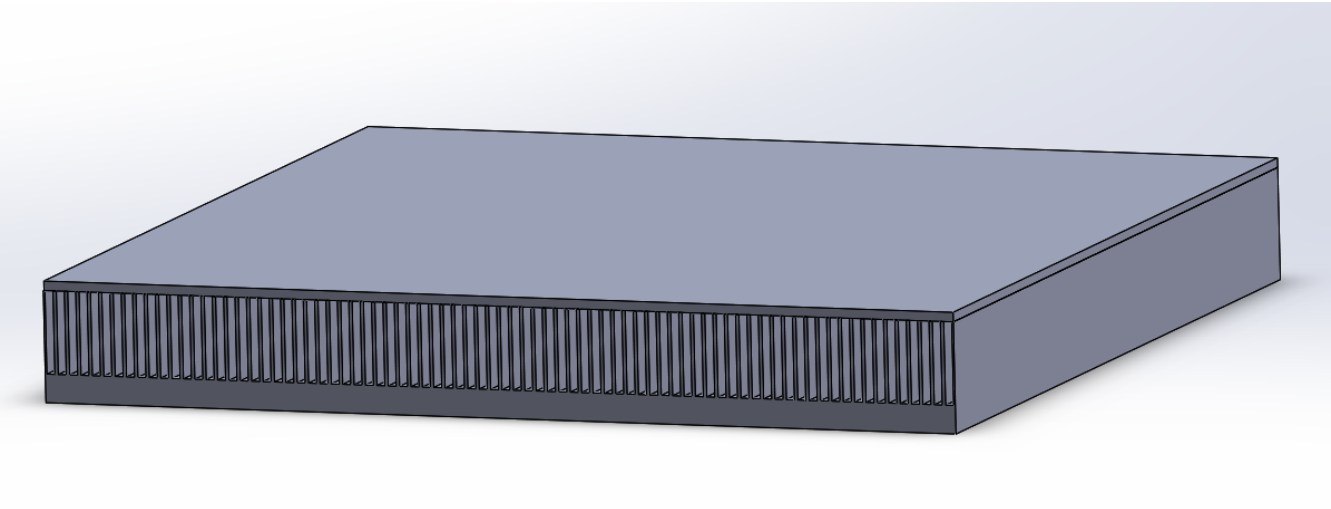

Atli Már Jónsson
Master Thesis. April 2019
Thermal Energy and Process Engineering

AALBORG UNIVERSITY
DENMARK

AALBORG UNIVERSITY
DENMARK

School of Engineering and Science
Energy Engineering
Pontoppidanstræde 111
9000 Aalborg
http://www.ses.aau.dk/

Title:

Techno-economic analysis of a heat sink for micro chip cooling

Project:

Master Thesis

Project period:

January 2019 - April 2019

Project author:

Atli Már Jónsson

Supervisors:

Thomas Condra
Alireza Rezaniakolaei

Pages: 71
Appendices: A
Project deadline: 22-4-2019

Abstract:

Thermal dissipation is essential to electronic devices to keep them working at their highest capability and to prevent them from malfunctioning. Electronic devices have become smaller and more powerful in recent years, leading to a higher rate of thermal dissipation occurring in a smaller area. A micro channel heat sink is a component that can be used to dissipate thermal energy from small electronic devices.

The rate of heat transfer through a heat sink is highly influenced by the design of it. The present paper presents a techno-economic analysis of several micro channel heat sink designs and focuses on determining the optimum design in regards to thermal performance and purchasing price. Simulations of the designs are conducted in Computational Fluid Dynamics (CFD) with a uniform heat flux and a fixed pumping power as operating conditions. The thermal resistance of multiple designs is compared and additionally set in relation to the purchasing price from an exemplary manufacturer.

The analysis showed a decreasing thermal resistance within the heat sink at an increasing number of channels incorporated in the design. However, at one point, the analyzed heat sinks' purchasing prices rise disproportionally compared to a neglectable increase of their thermal performance. The optimal micro channel heat sink design in regards to both thermal dissipation and purchasing price was identified to have 50 channels and a 0.7 width ratio between channels and fins.

Preface

This study was completed within the context of the Master of Science program in Energy Engineering specializing in Thermal Energy and Process Engineering at the Department of Energy Technology at Aalborg University. It represents the author's master thesis.

Acknowledgements

Writing this thesis would not have been possible without the support of several parties. Therefore, i would like to thank everyone that supported me within this process and made the research of this topic possible.

I would would like to give special thanks my supervisors, Alireza Rezaniakolaei and Thomas Condra, as they provided me with excellent guidance and constant feedback.

Aalborg University, April 22, 2019

Nomenclature

Abbreviation	Explanation
AAU	Aalborg University
CFD	Computational Fluid Dynamics
CPU	Central Processing Unit
IGBT	Insulated Gate Bipolar Transistor
MCHS	Micro Channel Heat sink
VLSI	Very Large Scale Integration
TDMA	Tri-Diagonal Matrix Algorithm

The following list of symbols are listed in a alphabetical order, followed by Greek letters.

Symbol	Explanation	Unit
A	Area	m^2
C	Cost	\$
c_p	specific heat	$W\,kg^{-}1\,K^{-}1$
D_h	Hydraulic diameter	m
f	Friction factor	−
fr	Frequency	$s^{-}1$
H	Height of a channel	mm
L_x	Length on x-plane	mm
L_y	Length on y-plane	mm
L_z	Length on z-plane	mm
L_e	Entry length	mm
L_c	Cross-cut length	mm
N	Number of channels in a heat sink	−
N_c	Number of cross-cuts	−
P	Pressure	Pa
$\dot{Q}$	Heat transfer rate	W
$\dot{Q}_{cond}$	Rate of heat transfer through conduction	W
$\dot{Q}_{conv}$	Rate of heat transfer through convection	W
$\dot{q}$	Heat flux	$W\,m^{-2}$
R_t	Thermal resistance	$K\,W^{-1}$
Re	Reynolds number	−
Re_{cr}	Critical Reynolds number	−
T	Temperature	K
$\overline{T}$	Mean fluid temperature	K
t	time	s
V	Volume	m^3
$\dot{V}$	Volumetric flow rate	$m^3\,s^{-1}$
$\vec{V}$	Velocity vector	−
v	Velocity	$m\,s^{-1}$
v_{mean}	Average velocity	$m\,s^{-1}$
v_{max}	Maximum velocity	$m\,s^{-1}$

Symbol	Explanation	Unit
W	Width of the heat sink	mm
w_c	Channel width	mm
w_f	Fin width	$\mathrm{m\,s^{-2}}$
w_p	Pitch width	mm
α	aspect ratio	–
β	Width ratio	–
η_{fin}	Fin efficiency	–
μ	Viscosity	$\mathrm{kg\,m^{-1}s^{-1}}$
ρ	Density	$\mathrm{kg\,m^{-3}}$
Γ	Diffusion coefficient	–

Contents

Introduction and Motivation

1

Heat transfer processes are surrounding us in our every-day life. One example is the process of boiling an egg in a pot of water. The water needs to reach a boiling point with a transfer of heat from the stove, for the egg to become hard on the inside.

But heat transfer processes can not only be observed all around us, they also play a crucial role in our society. Their understanding is critical for various field, such as medicine, meteorology, or architecture, to mention but a few. They also become increasingly important for maximizing the energy efficiency of industrial activities and to replace fossil fuels with clean energy sources [Shafiee and Topal, 2009]. For the field of energy engineering in general, heat transfer processes are indispensable.

The invention of electricity represented a big leap in technological progress, with a rapid development of electronic devices over the 20th century [Whitfield, 2008]. In recent years, electronic devices have become a major part of everyday life, as they can be found in almost every business and household around the world. As the world evolved, new technologies were developed, and devices have become smaller and more efficient [Smith et al., 2014]. Those devices can generate a high amount of thermal energy, which have to be dissipated away from the electronic device, to prevent it from overheating, as this would lead to malfunctioning. A first application for electronic device cooling can be found in early US Navy documents [WELSH, 1954].

Heat sinks can facilitate electronic device cooling. A heat sink is a heat exchanger, which is attached to mechanical or electronic devices, where it dissipates heat from the devices by exposing a larger area of material to the cool surroundings [Çengel, 2011].

Increased malfunctioning of electronic devices through insufficient heat transfer performance in heat sinks is connected to a lower efficiency in the use phase of these devices. It can also mean shorter lifespans of these electronic products and

an increased number of repairs - both leading to additional energy and resource use. This represents a particular pressing issue, as emissions and waste have been growing in line with the increased extraction of natural resources [United Nations Department of Economic and Social Affairs, 2017] and resources used in the production of electronic devices such as aluminum, copper, and other kinds of metals are becoming more and more scarce as the demand for those resources increases every year [Treadgold, 2018]. Shorter lifespans and repairs also mean increased costs for the user of these electronic products. Improving the performance of heat sinks for electronic products would thus have positive impacts on the environment and minimize the consumption of resources.

A factor important for the electronics market is not only the thermal performance but also the size of components like a heat sink, as the demand from a modern consumer is to have compact and efficient electronic devices. With a reduction of the electronic devices in size the power density increases, and dissipating thermal energy from the electronic devices with efficient and compact cooling solutions becomes harder. For purchasers, there is not only a focus on minimizing size and increasing the heat transfer performance of the heat sinks, but also on keeping the purchasing costs low. A high user demand for affordable products in a competitive and highly globalized electronics market makes the cost-efficiency of components a focus for manufacturers.

This study aims at finding an optimal design considering price and performance of a specific type of heat sink in a given size: An aluminum straight micro channel rectangular heat sink. Due to the high use of this kind of heat sink for several electronic products, the optimization of costs and performance is highly relevant.

To identify this optimal design, first an overview of state of art literature focusing on micro channel heat sinks is given (CH. 2). Building on the state of art, the aim of the present study is introduced (CH. 3). The following chapter (CH.4) then focuses on the theoretical basis the analysis builds upon. It gives an overview of the basic heat transfer mechanisms, and fluids flow and heat transfer in a channel, before laying the theoretical groundwork for the finite volume method and optimum design determination. Subsequently, the methodologies used in the present paper are described (CH. 5), including methods for the design optimization, cost analysis, and modelling simulations. The results of the analysis are presented (CH. 6) and discussed (CH. 7), before a summary of insights and an outlook into further research is given in the conclusion (CH. 8).

State of the art

2

This chapter gives an overview of the current state of art of the research field that concerns heat sink designs (CH. 2.1). It addresses designs with different cooling mediums (CH.2.2), including air cooling as well as liquid cooling.

2.1 Heat sink design

To cool electronic devices, heat sinks transfer heat generated by the device to a medium. The heat sink can absorb or dissipate thermal energy from this medium to cool or warm up an adjacent device [Hamburgen, 1986]. A micro channel heat sink is displayed in figure 2.1.

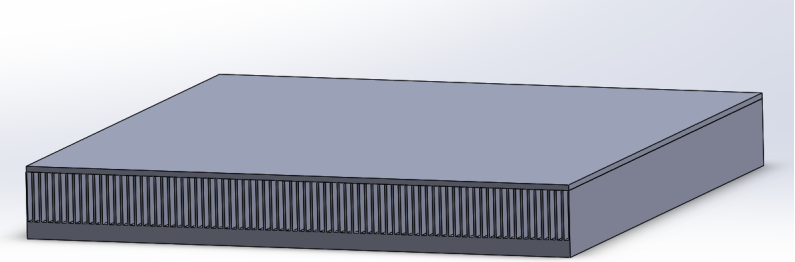

Figure 2.1: Rectangular micro channel heat sink with 80 channels

Purchasers of heat sinks take into consideration the size, thermal performance, and cost of a heat sink when making a purchasing decision. The physical properties and the design of a heat sink can have a big impact on the latter, as material choices, but also each cut for a channel can rapidly increase the cost in the production [Lee, 1995].

Most studies within this field focus on improving the heat sink design for high thermal performance [Li and Peterson, 2006; Saini and Webb, 2002; Li and

Peterson, 2007], often through maximising the area of the surface that is in contact with adjacent fluid [Hamburgen, 1986].

Figure 2.2 gives an overview of design variables, which refer to the physical properties of a heat sink.

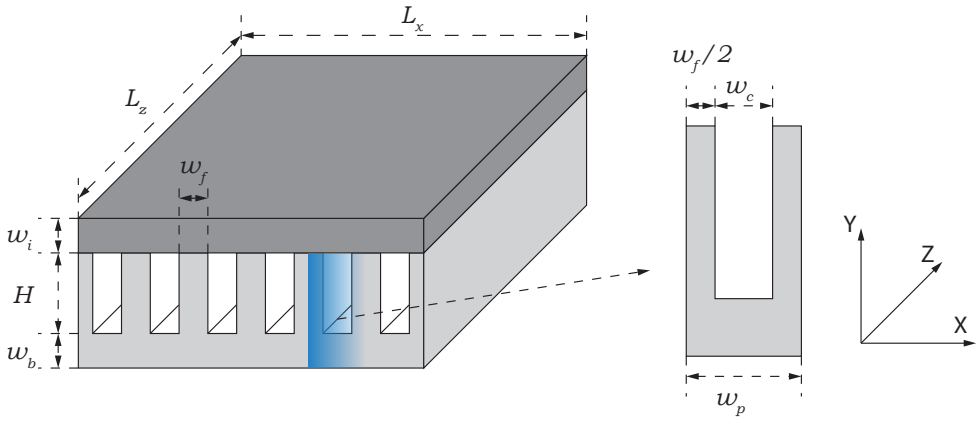

Figure 2.2: Design variables in a heat sink

L_z and L_x describe the lengths that make up the heat sink area (A). H defines the height of the channels. w_i is the width of the insulation material on top of the heat sink, and w_b is the width of the base area below the heat sink. Together, w_i, H, and w_b make up the entire height of the heat sink. w_f is the width of a fin. Fins are the columns which are between the channels in a heat sink. The image next to the whole heat sink in figure 2.2 shows a segment of the heat sink called a pitch, which is often used as a unit of analysis. The width of this pitch (w_p) is made up of one channel width (w_c) and two half fin widths (2 x $w_f/2$). Usually, the heat to be dissipated, arrives at the bottom of the heat sink. The medium used for heat transfer enters the channel entrances visible in the illustration. These are called the inlets. The medium leaves on the channel outlets at the opposite side of the heat sink.

2.2 Cooling media

Liquids or gases can be used as a medium that is transferring the heat in a heat sink. Water and other liquids are more ideal options for heat transfer, as they typically

have better heat transfer capabilities than gases [Çengel, 2011], and are thus used for many high power electronics [Zhao and Lu, 2002].

2.2.1 Air cooling

Numerous studies have been conducted thematizing air-cooled heat sinks [Zeng et al., 2018; Katoh et al., 2004; Rodgers and Eveloy, 2013]. Saini and Webb [2002] studied the heat rejection limits of air-cooled plane fin heat sinks used for cooling Central Processing Units (CPUs), considering both duct flows and impinging flows.

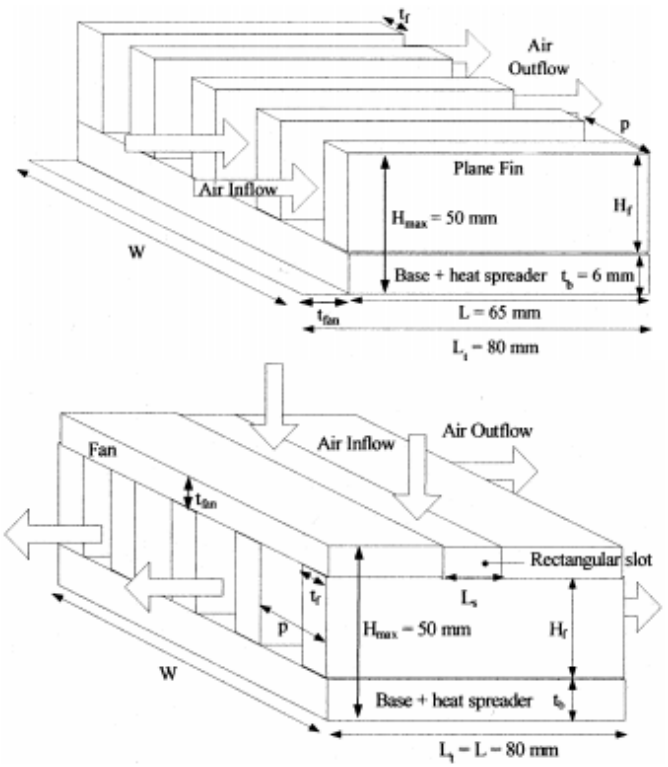

Figure 2.3: Duct flow (top) and impinging flow (bottom) coming into a heat sink [Saini and Webb, 2002]

As illustrated in figure 2.3, a duct flow is a flow of air that comes into the heat sink from one side and then travels horizontally to the outlet of the heat sink. An impinging flow describes a flow of air that comes into the middle of the heat sink vertically from the top, where the air is then distributed to both sides of the

heat sink horizontally. An impinging flow comes in normal direction to the surface that is being cooled, unlike the duct flow that flows adjacent to the surface [Marzec and Kucaba-Pietal, 2014]. In the study by Saini and Webb [2002], heat transfer in heat sinks with different base areas were compared for both duct flow and the impinging flow case. The base areas analyzed were 80×60 mm and 80×80 mm (also illustrated in figure 2.3). The heat sink base area of 80×80 mm resulted in a better heat distribution, indicating that bigger heat sink area is beneficial to the thermal distribution.

An optimization method was used for the other parameters. These were set within a certain range. For the duct flow case, the height of the fin (H) was set in the range of 15-44 mm, the fin width (w_f) was 0.3-1.2 mm, and the pitch width (w_p) was 1-3.6 mm. The limits of the parameters in the impinging flow case were in the range of 15-29 mm for the fin height (H), 0.2-1.2 mm for fin width (w_f), and 1-3.5 mm for the width of the pitch width (w_p).

Table 2.1: Results for both duct and impinging flows for an optimum sized heat sink

Flow	Increase in fan speed (%)	H (mm)	w_p(mm)	w_f(mm)	ΔP(Pa)	R_t(K/W)	$\dot{Q}$(W)
Duct flow	0	44	2.7	0.9	17.63	0.416	84
	5	44	2.7	0.9	19.08	0.408	85.8
	10	44	2.4	0.7	20.57	0.399	87.7
	15	44	2.4	0.7	22.07	0.392	89.4
	20	44	2.4	0.8	25.75	0.385	91
	25	44	2.4	0.8	27.52	0.378	92.6
Impinging flow	0	29	1.5	0.3	16.54	0.371	94.4
	5	29	1.5	0.3	17.84	0.363	96.5
	10	29	1.5	0.3	19.18	0.355	98.5
	15	29	1.5	0.3	20.57	0.349	100.2
	20	29	1.5	0.3	22	0.344	101.8
	25	29	1.5	0.3	23.48	0.338	103.4

As can be seen in table 2.1, the optimum parameters for H, w_p, and w_f at different fan speeds are listed. The highest heat transfer in the duct flow case was 92.6 W, occurring at a 25 % increase in fan speed. The highest heat transfer ($\dot{Q}$) in the impinging flow case was 103.4 W and was encountered at an increasing fan speed of 25 %. It also shows a lower pressure loss than the same fan speed in the duct flow [Saini and Webb, 2002].

2.2.2 Liquid cooling

The first study aiming at identifying the optimal design of a micro channel heat sink was conducted by Tuckerman and Pease [1981]. Their study focused on the theoretical as well as the experimental performance of micro channel heat sinks, with the coolant fluid being water. The aim of the research was to find the optimum design variables for the channel width (w_c), fin width (w_f), and the aspect ratio (α) between H and w_c for minimum thermal resistance through the micro channel.

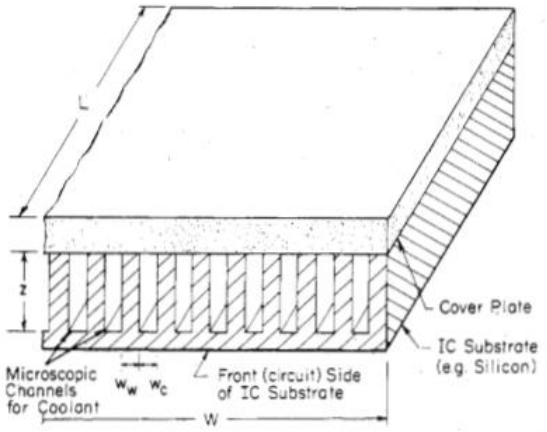

Figure 2.4: Schematic view of a compact heat sink incorporated into an integrated circuit chip [Tuckerman and Pease, 1981]

The study focused on High-Performance Heat Sinks for Very-Large-Scale Integration (VLSI), where the liquid flow comes into the rectangular finned channel. The heat source from the VLSI was uniformly distributed along the cold plate with an area of 100 mm^2. Silicon substrate was used as a material for the micro channel heat sink.

The variables used in the experimental part of the study can be seen in table 2.2, where all the experiments have similar parameters and the maximum thermal resistance was around 0.1 K/W for area of 100 mm^2 in all experiments.

Table 2.2: Experimental values [Tuckerman and Pease, 1981]

Expt	w_c(mm)	w_f(mm)	H(mm)	$\dot{V}$(m^3/s)	R_t(K/W)	$\dot{q}$(kW/m^2)
1	0.056	0.044	0.320	$4.7{\cdot}10^{-6}$	0.110	1800
2	0.055	0.045	0.287	$6.5{\cdot}10^{-6}$	0.113	2800
3	0.050	0.050	0.302	$8.6{\cdot}10^{-6}$	0.090	7900

$\dot{V}$ is the volumetric flow rate, R_t is the thermal resistance, and $\dot{q}$ is the heat flux.

It was concluded in this study that microscopically narrow channels with high aspect ratio are the best design for an efficient heat removal, where it can dissipate up to 13000 kW/m^2.

Since 1981, numerous theoretical and experimental studies have been conducted with geometrical optimization of micro channel heat sinks. Sasaki and Kishimoto [1986] investigated the heat sink's cooling ability and the channel width with a constant pressure loss in the micro channels. Knight et al. [1992b] proposed an optimization of heat sinks with forced convection for three different fin array design of 6, 9, and 12 channels with the same pressure loss across the channels.

In 2006, Li and Peterson [2006] examined geometric optimizations of a micro channel heat sink with liquid flow, with a numerical simulation of the fluid flow through the micro channel of the heat sink. The area of the heat sink was 100 mm^2, with a width of the base w_b of the heat sink at 0.9 mm, height of the channel at 0.180, and 0.360 (mm) for a number of channels (N) in the heat sink ranging from 40 to 140.

Table 2.3: Values of parameters for an optimal geometry analysis for channel height of 180 mm and 360 mm [Li and Peterson, 2006]

H(μm)	N	β	D_h(mm)	ΔP(Pa)	$\bar{u}_m$(m/s)	Re	L_e(mm)	L$_e$/L_z	R_t (K/W)
360	40	0.7	0.235	9866	2.01	544	6.4	0.64	0.251
	60	0.6	0.156	17008	1.36	244	1.9	0.19	0.185
	80	0.7	0.141	17755	1.12	180	1.2	0.12	0.167
	100	0.7	0.117	21805	0.91	122	0.7	0.07	0.162
	120	0.7	0.100	25882	0.76	88	0.44	0.044	0.156
	140	0.8	0.098	24688	0.7	79	0.38	0.038	0.184
180	60	0.7	0.141	22668	1.75	284	2	0.2	0.297
	80	0.7	0.117	27906	1.42	192	1.1	0.11	0.252
	100	0.8	0.110	27996	1.24	158	0.87	0.087	0.233
	120	0.8	0.097	32485	1.06	119	0.58	0.058	0.223
	140	0.8	0.086	37049	0.93	93	0.4	0.04	0.225

Table 2.3 summarizes the results of this study. H describes the height of the channel, N is the number of channels, β is the width ratio, and D_h is the hydraulic diameter. ΔP is the pressure loss across the channel, $\bar{u}_m$ is the fluids mean velocity,

Re is the Reynolds number, L_e is the length for a fully developed flow, L_z is the length of the channel, and R_t is the thermal resistance.

Multiple numerical studies have been conducted with the focus on optimizing different characteristics of the rectangular micro channel heat sink. For example, Bello-Ochende et al. [2007] scrutinized the optimal aspect ratio that minimized the maximum temperature of a micro channel heat sink with fixed volume of $0.9 \cdot 10^{-10}$ m ^{3} and axial length of 10 mm.

Ermagan and Rafee [2018] investigated rectangular micro channel heat sinks' (MCHS) optimal geometry for different channel wall surfaces. The study on the thermal performance of the MCHS was performed numerically. The aim was to minimize thermal resistance with a optimal geometry of a heat sink at a constant pumping power, for three different wall hydrophobicities, namely a conventional wall (polar), a hydrophobic wall (non-polar), and a superhydrophobic wall (non-polar). The aim of the research was to determine if hydrophobic walls or superhydrophobic walls have less overall thermal resistance than conventional walls. The model included a heat sink area of A 10 x 10 mm and a constant uniform heat flux of 1000 kW/m^2. The height of the heat sink was fixed at 0.9 mm and the channel height had two different values: 0.360 mm and 0.700 mm.

Table 2.4: Optimal values of geometrical and flow parameters [Ermagan and Rafee, 2018]

H(μm)	Wall surface	l_s	β	N	w_c(mm)	D_h(mm)	Re	R_t (K/W)
	Convential	0	0.714	80	0.089	0.143	173.17	0.198
360	Hydrophobic	1	0.711	80	0.088	0.142	171.638	0.188
	Superhydrophobic	20	0.679	140	0.048	0.085	115.178	0.159
	Conventional	0	0.654	80	0.081	0.146	133.556	0.156
700	Hydrophobic	1	0.652	80	0.081	0.146	132.608	0.147
	Superhydrophobic	20	0.615	140	0.043	0.082	85.504	0.129

The results from this study are displayed in table 2.4. The authors reached the conclusion that the hydrophobic and superhydrophobic wall reduced the thermal resistance by 5 and 20 %, respectively.

The conventional micro channel heat sink employs straight channels with nearly constant streamlines in the fluid, which according to Çengel [2011] will lead to a low heat transfer due to the poor mixing of fluid and an increased thermal boundary layer along the channel. A possible solution to this problem is the em-

ployment of different shaped fins. Studies on heat sinks with different shape of fins have been conducted, addressing wavy fins [Sui et al., 2010], pin fins [Peles et al., 2005], Y-shaped [Kim, 2014] and T-shaped fins [Hazarika et al., 2016]. Many other different shapes and applications of heat sinks can be found in the review paper by Ahmed et al. [2018].

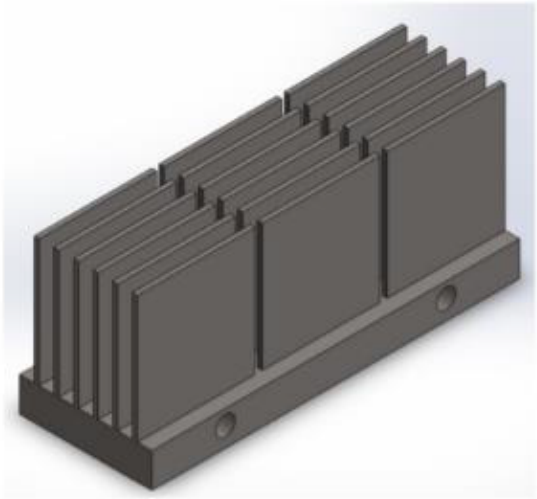

Figure 2.5: Cross cut heat sink [Chingulpitak et al., 2016]

Cross cut heat sinks, which have gaps in the fins along the length of the heat sink, were investigated numerically and experimentally by Chingulpitak et al. [2016]. The author investigated the effects of cross-cut lengths (L_c) and number of cross-cuts (N_c) along the length of a heat sink with 5 channels. The geometric profile of the heat sink was a fixed value of 27 mm at the width of the cold plate (L_x), 25 mm for the height of the fins (H), 0.5 mm for width of the base (w_b), 1 mm for width of the fin (w_f) and 3 mm for width of the channel. For the experiment, numerous values were used for the number of the cross-cuts (N_c)(2 mm, 4 mm and 6 mm) and their length (L_c) (0.5 mm, 1 mm, 1.5 mm, 2 mm, 3.5 mm and 4mm). The study was focused on the effects that number and length of cross-cut had on Reynolds number, thermal resistance, and pressure loss at constant pumping power (the power used to move the fluid throughout the heat sink).

It was concluded that a cross cut length of 1.5 mm had the lowest thermal resistance, whereas the optimum length for thermal resistance was identified to be somewhere between 1.5 and 2 mm. At a cross cut heat sink width (N_c) value of 6

mm and length (L_c) value of 1.5 mm, the thermal resistance was 16.2 % lower than in a plate fin heat sink with the same pumping power.

Research Objective

3

The summary of the state of art of research on heat sink design revealed that a large number of studies has been conducted on the thermal performance of numerous designs of heat sinks. The importance of an optimal design of a heat sink for the highest possible heat transfer is a clear red threat in the conducted research. While heat sinks and heat transfer is a well researched area, the relationship between design, thermal performance, and cost of heat sink designs is a combination less considered in current literature.

The present research aims at addressing this gap by first identifying thermal performances of different designs of a rectangular micro channel heat sink and then putting these performances in relation to the purchasing cost. The conducted study aims at improving information on the cost of customized heat sinks compared to the thermal dissipation by answering the research question: *"What is the optimal design of a rectangular micro channel heat sink, in terms of heat distribution and purchasing cost?"*

Certain design variables and operating conditions were chosen to narrow down the scope of the conducted analysis. Design variables included a fixed area of the heat sink, fixed height, and aluminium as a material choice, while operating conditions included a fixed pumping power, a uniform heat flux, and a constant temperature at the inlet of the fluid flow. Moreover, for the simulation of the present study, the analyzed heat sink was assumed to be attached to an Insulated Gate Bipolar Transistor (IGBT) micro chip, presenting the source of heat to be dissipated by the heat sink. Tests of all geometries in a steady state of heat flux were conducted in order to determine which design of a heat sink had the highest thermal distribution.

Furthermore, the optimal design in terms of both thermal distribution and cost was simulated in a transient state of heat flux, to see if the fluctuation of temperature in a channel does not exceed operating temperature limit of the IGBT at 423 K [Fairchild Semiconductor Corporation, 2008].

Theoretical Background

4

This chapter lays the theoretical basis for this work by introducing general mechanisms of heat transfer (CH. 4.1), theory on the development of fluid flow in a channel (CH. 4.2), the numerical method of finite volume (CH. 4.3) and optimisation theory (CH. 4.4).

4.1 Heat transfer mechanisms

Heat is defined as an energy that can be transferred between mediums, if there is a difference in temperature between the mediums. The higher temperature medium always transfers heat to the lower temperature until they reach thermal equilibrium [Bergman et al., 2011]. There are three different ways of heat transfer, namely conduction, convection, and radiation [Kreith et al., 2012]. In the present study, radiation will be neglected and the focus will be on conduction and convection in the following sections.

4.1.1 Conduction

Conduction is a heat transfer mechanism that can transport thermal energy in materials from the high temperature side of the material to the cold one. Mediums in which a conduction can take place can be solid, liquid, or gaseous. For a medium to be able to allow conduction through it, there must be no forced movement of the medium, as this would be considered convection [Welty et al., 2009] (see 4.1.2).

Conductivity is measured in Watt per meter Kelvin (W/mK). Solid materials have in most cases better conduction than liquids and gases, even though some insulation materials such as fiberglass and cork have lower conduction than some liquids and gases [Powell et al., 1966].

Table 4.1: Thermal conductivity of common solid materials and fluids at 298 K [Mills, 1992]

Elements	k (W/mK)
Aluminum	204
Copper	386
Mild Steel	64
Water	0.611
Engine oil	0.145
Air	0.027

Table 4.1 shows materials that are often used in applications for heat transfer.There are many parameters that can influence the rate of heat conduction from one medium to another. The most influential parameters are:

- Geometry
- Thickness
- Material selection
- Temperature difference

Every parameter plays an important role in getting the best thermal conduction across a medium. With a steady heat conduction through a medium, the rate of heat transfer can be determined with the following equation:

$$\dot{Q}_{cond} = \frac{k}{L} A \Delta T \tag{4.1}$$

k equals thermal conductivity, A is the cross sectional area, L is the length of a medium, and ΔT is the temperature difference between each sides of the medium [Mills, 1992].

4.1.2 Convection

An energy transfer between a solid surface and a flow in a liquid or gaseous medium is called convection. Convection is a combination of both conduction (see 4.1.1) and fluid motion. Thus, the convection is reliant on a fluid motion, whereas a heated solid surface without fluid motion is only effected by conduction [Çengel, 2011].

The heat transfer through forced convection can be enhanced with a higher rate of velocity of the fluid flow in contact with a solid surface. Forced convection is a heat transfer through motion of a fluid in a contact with a solid surface, where a outside force is responsible for the fluid motion [Mills, 1992].

Natural convection does not rely on a outside force for the transfer of heat between the fluid and the solid surface. The motion of the fluid in natural convection is due to the difference in density as heat is coming into the media [Kays, 2012].

Table 4.2: Common values of convection heat transfer coefficients [Çengel, 2011]

Type of convection	$h(W/m^2K)$
Natural convection of gases	2-25
Natural convection of liquids	10-1000
Forced convection of gases	25-250
Forced convection of liquids	50-20000
Boiling and condensation	2500-100000

The rate of heat transfer $\dot{Q}$ by convection is formulated as,

$$\dot{Q}_{conv} = hA_s \left(T_s - T_\infty\right) \tag{4.2}$$

h is the convection heat transfer coefficient, A_s is the surface area where convection takes place, T_s is the temperature of the solid surface, and T_∞ is the temperature of the surrounding medium [Çengel, 2011].

The rate of heat transfer through convection is influenced by the geometry of the solid surface, properties of the fluid being used as a coolant, flow regime in the fluid, and the amount of heat flux coming into the fluid medium from the solid surface. Some geometries, such as a rectangular heat sink, rely heavily on the efficiency of the fins in the channels of the heat sink to gain the highest heat transfer through convection [Hamburgen, 1986].

4.1.3 Contact resistance

A rough surface can create a contact resistance at an interface between two adjacent solid media. The rough surface creates insulation with multiple air holes at the interface of the solid media which can cause a temperature change in the heat transfer through the interface [Çengel, 2011].

Most theoretical studies do not account for a temperature change at an interface between two solid media and work with the assumption that there is no contact resistance between the media. However, real life situations always have some contact resistance, as there is always some temperature change between two contact layers [Mills, 1992].

Materials have different roughness at their surface, which has a big effect on the heat transfer going through two adjacent solid media.

Table 4.3: Typical interfacial conductance at a moderate pressure [Mills, 1992]

Interface	h_c (W/m^2K)
Ceramic-ceramic	500-3000
Ceramic-metals	1500-8500
Graphite-metals	3000-6000
Stainless steel-stainless steel	1700-3700
Aluminum-aluminum	2200-120000
Stainless steel-aluminum	3000-4500
Copper-copper	10000-250000
Rough aluminum-aluminum (vacuum conditions)	≈150
Iron-aluminum	4000-40000

The thermal contact resistance R_t is the resistance of the heat transfer in the interface, where the thermal resistance is divided by the whole nominal contact area.

$$R_t = \frac{1}{h_c} = \frac{\Delta T_{interface}}{\dot{Q}/A} \tag{4.3}$$

h_c is thermal contact conductance, A is the apparent interface area, and $\Delta T_{interface}$ is the effective temperature difference at the interface [Çengel, 2011].

In this study, the assumption is that the contact between surfaces is perfect and that there is no thermal contact resistance, as it is difficult to measure the contact resistance between solids, as the wide range in (see Table 4.3) indicates.

4.2 Fluid flow and heat transfer in a channel

The flow regime and the rate of heat transfer for an internal fluid flow in a channel can develop in different ways, depending on the geometry and the boundary conditions set for a channel in a heat sink [Çengel, 2011].

An internal flow in a rectangular channel has viscous forces exerted upon it immediately at the inlet of the channel. The viscous forces are due to the no slip condition [Prabhakara and Deshpande, 2004] from the adjacent wall to the fluid flow in a channel. They create a boundary layer in the fluid flow, where the thickness of the boundary layer increases with the length of the channel until it reaches the center of the channel, where the boundary layer will cover the whole channel. A Fully developed flow is established in a channel when all of the fluid flow has been exposed to viscous forces and velocity of the fluid flow stays constant along the channel [Ferrás et al., 2012].

The length of the channel before a flow is considered to be fully developed, and is called hydrodynamic entry length L_e ,

$$L_{e,\quad laminar} \approx 0.05 Re D_h \tag{4.4}$$

Re is the Reynolds number and D_h is the hydraulic diameter in an internal rectangular channel [Cengel, 2010].

4.2.1 Velocity profile

The thickness of the boundary layer for a fully developed laminar flow in a circular pipe, grows at the same rate, because the pipe is symmetric in all directions from the center line. If the aspect ratio α of a rectangular channel is bigger than 1, the velocity profile does not grow simultaneously like in pipe or square duct [Husain and Kim, 2008].

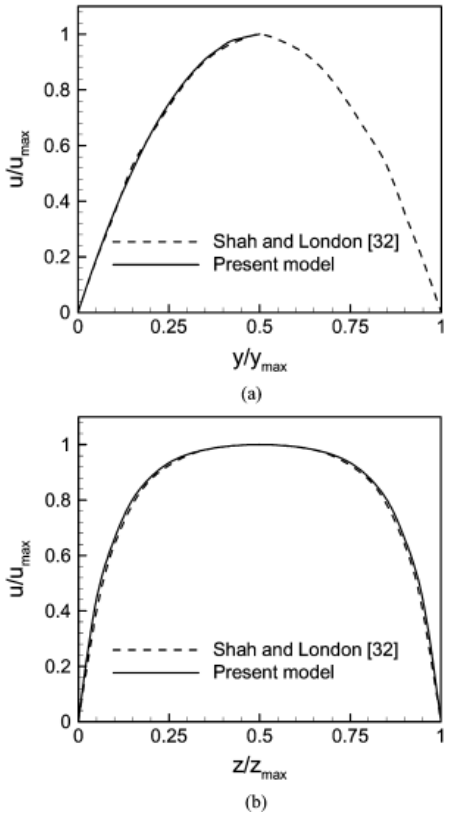

Figure 4.1: Velocity profile at mid plane of width and height in a channel [Husain and Kim, 2008]

Figure 4.1 shows the velocity profile at a cross-sectional plane cut through the height and the width of a rectangular channel. y/y_{max} is taken from the middle plane through the width of the channel w_c and Z/Z_{max} is taken from the middle plane through the Height H of the channel. The U/U_{max} is the velocity at all points in the profile. The maximum velocity in a rectangular channel can be acquired by using the following equation,

$$v_{max} = 1.5 \cdot v_{mean} \tag{4.5}$$

v_{max} is the maximum velocity in the channel, v_{mean} is the average velocity in the channel, and 1.5 is a fixed value to acquire the maximum velocity for the rectangular channel [Dou, 2005]. The width and height of a rectangular micro channel differ. That is why the standard equation for the velocity profile in a pipe cannot be used to describe the velocity profile along the length of rectangular channel. In a study by Zheng and Silber-Li [2008], the theoretical velocity profile

is described along a rectangular channel in a fully developed flow with an equation from White [1974].

$$u_x(y,z) = \frac{4H^2\Delta P}{\pi^3\mu L}\cdot\sum_{n=1,3,5...}^{\infty}\left[1-\frac{\cosh(n\pi\frac{y}{H})}{\cosh(n\pi(\frac{w_c}{2H})}\right]\sin(n\pi\frac{z}{H}) \tag{4.6}$$

H is the height, w_c is the width, and L is the length of the channel. ΔP is the pressure loss in the channel along length L. The term n is used to get more accuracy for the polynomial part of the equation. The n increases after each iteration until there are no changes in results between iterations.

4.2.2 Temperature profile

Theoretical calculations of a temperature profile are often unreliable, as convection in a channel is very hard to predict due to its complexity [Mills, 1992]. Literature from 2014 by Rybiński and Mikielewicz [2014] discusses an analytical solution of heat transfer in rectangular channels in a laminar flow. The temperature profile was made two terms in explicit form, where laminar flow asymptotic solution between parallel plates was the first term and rapidly convergent series were the second term.

The wall temperature T_w is assumed to be uniform along the adjacent area of the solid to the fluid medium in an isothermal state, as the heat flux coming into the channel is considered to be constant in z-direction. The temperature profile can be assessed with following equation [Rybiński and Mikielewicz, 2014].

$$\begin{aligned} T(x,y) = T_w + \frac{\rho c_p}{k}\frac{d\bar{T}}{dz}\frac{1}{\mu}\frac{dp}{dz}\frac{1}{8}\left(\frac{y^4}{3}-\frac{h^2y^2}{2}+\frac{5h^4}{48}\right) \\ +2h^4\sum_{n=1}^{\infty}\frac{(-1)^n}{u_n^5}\left[2+u_n\alpha\frac{1}{2}\tanh\left(u_n\alpha\frac{1}{2}\right)-u_n\alpha\frac{x}{w}\tanh\left(u_n\alpha\frac{x}{w}\right)\right] \\ \times\frac{\cosh\left(u_n\alpha\frac{x}{w}\right)}{\cosh\left(u_n\alpha\frac{1}{2}\right)}\cos\left(u_n\frac{y}{h}\right) \end{aligned} \tag{4.7}$$

$$u_n = (2n-1)\pi \tag{4.8}$$

k is the thermal conduction, c_p is the specific heat of the fluid, and $\bar{T}$ is the mean fluid temperature. The n in the rapidly convergent series in equation 4.8 increases after each iteration until there are no changes in results between iterations, like in Eq. 4.6. To find an asymptotic solution between parallel plates of a fully developed laminar flow in the channel, the Poisson equation is used.

$$\frac{\partial^2 v}{\partial x^2} + \frac{\partial^2 v}{\partial y^2} = \frac{1}{\mu}\frac{dp}{dz} \tag{4.9}$$

The properties of the fluid are considered to be constant as the temperature is neglected as Eq. 4.9 in the derivation from the Navier-Stokes equation [Rybiński and Mikielewicz, 2014].

4.2.3 Critical Reynolds number for a rectangular channel

The Reynolds number Re is a dimensionless number that describes the ratio between inertia forces and viscous forces in the fluid. Parameters of a solid area and properties of a fluid are used to determine the Re as a criterion to differentiate laminar flow from turbulent [Gerhart et al., 2016]. The critical Reynolds number Re_{cr} is the highest Re that a fluid flow can be at while still being considered a laminar flow [Cengel, 2010].

Re_{cr} for a internal flow in a square channel is 2300 [Kiijarvi, 2011]. The Re_{cr} for rectangular channels changes as the aspect ratio between height H and width w_c of the channel increases.

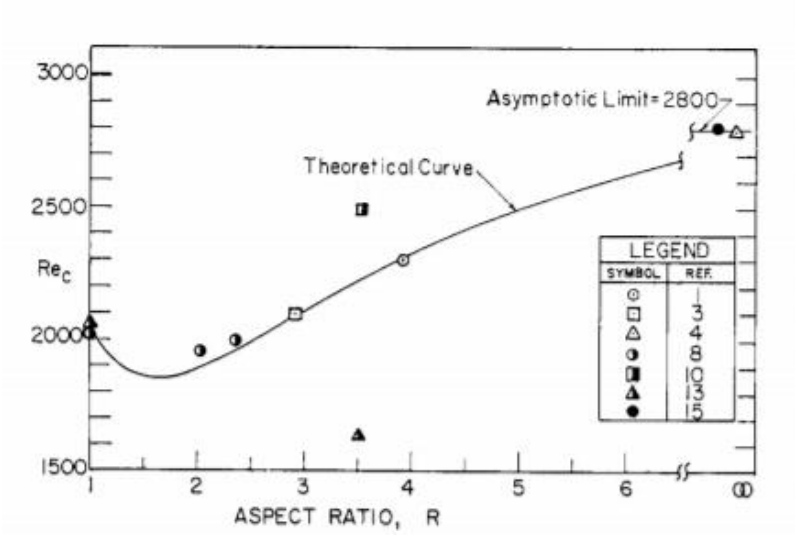

Figure 4.2: Critical reynolds number at different aspect ratios [Hanks and Ruo, 1966]

A study from Hanks and Ruo [1966] made a theoretical curve for a critical Reynolds number for channels at different aspect ratios, as can be seen in figure 4.2. The theoretical data from a previous study was compared with data from experiments at the same aspect ratio, showing that the data from the theoretical calculation was in line with the data from the experiments.

Table 4.4: Re_{cr} of different aspect ratios [Hanks and Ruo, 1966]

α	Hanks and Ruo (1966)
1	2060
2.04	1900
2.36	1960
2.92	2085
3.92	2315
>10	2800

The results from table 4.4 show that the critical Reynolds number takes a little slope downwards as the aspect ratio goes from 1 to 2. Beyond the aspect ratio of 2, the critical Reynolds number rises almost linearly towards an aspect ratio of around 10. The highest critical Reynolds number is reached at the point where the aspect ratio is higher than 10 in a channel, where all channels with a aspect ratio higher then 10 will have Re_{cr} of 2800.

4.2.4 Pressure loss

The pressure loss in a channel or a pipe is determined by two factors; primary and secondary losses. The primary losses are due to the viscous forces that act as restraining forces between the solid and the fluid [Gerhart et al., 2016]. The pressure loss due to viscous forces in a fluid flow is expressed in the following equation.

$$\Delta P = f \frac{L}{D_h} \frac{\rho V_{avg}^2}{2} \tag{4.10}$$

f is the friction factor, L is the length of the channel, D_h is hydraulic diameter of the channel, ρ is the density of the fluid, and V_{avg}^2 is the average velocity of the fluid [Kiijarvi, 2011].

The friction factor for a laminar flow in a pipe, can be formulated as

$$f = 64/Re \tag{4.11}$$

The friction factor is a function of the Reynolds number, as the Re gets higher, the friction factor gets lower, resulting in less viscous effect on the fluid [Gerhart et al., 2016].

The friction factor in a turbulent flow can be estimated using the Blasius formula for smooth pipes at $Re > 4000$ [Kiijarvi, 2011].

$$f = \frac{0.316}{\sqrt[4]{Re}} \tag{4.12}$$

The transfer of mass, momentum, and heat is much greater in turbulent flows than in laminar flows, which gives higher values of friction in a turbulent flow [Cengel, 2010].

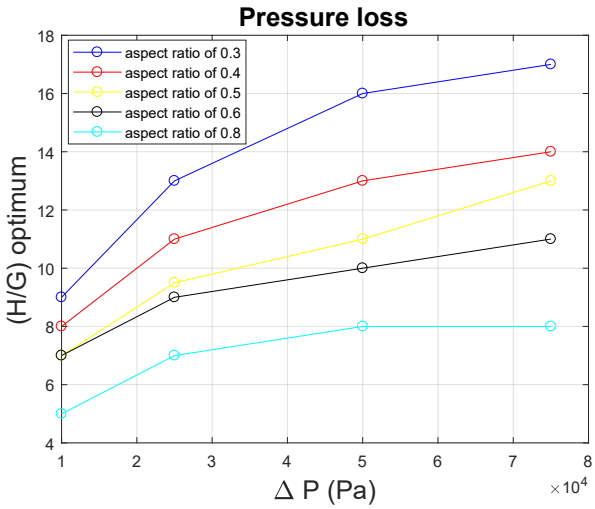

Figure 4.3: Pressure loss at different aspect ratios [Bello-Ochende et al., 2007]

The figure 4.3 shows results from a study of Bello-Ochende et al. [2007] for pressure loss at different diameters in a heat sink. The optimum ratio between the height of the channel (H) and the width of the channel and fin in the heat sink (G) was found for each individual aspect ratio α of the channels in regard to pressure loss.

Secondary losses are losses due to expansion, contraction, bends, valves, fittings, inlets and exits in the structure of the pipe or a channel [Kudela, 2010].

4.2.5 Fins in heat sinks

Extending the surface in contact with a fluid medium by placing fins onto the surface is a good way to enhance the heat transfer from a surface to a fluid medium. Fins can have a wide range of different geometries, such as rectangular, triangular, parabolic, circular, and pin fins [Lorenzini et al., 2011]. To find the efficiency of a fin, the following equation can be used.

$$\eta_{fin} = \frac{\dot{Q}_{fin}}{\dot{Q}_{fin,ideal}} \tag{4.13}$$

$\dot{Q}_{fin}$ is a fin's real heat transfer rate and $\dot{Q}_{fin,ideal}$ is a fin's ideal heat transfer rate [Çengel, 2011]. The heat transfer is uniform along the fin. The real heat transfer

of a fin can be found by adding η_{fin} to Eq. 4.2 for the following equation.

$$\dot{Q}_{conv} = hA_s\left(T_s - T_\infty\right)\eta_{fin} \quad (W) \tag{4.14}$$

η_{fin} can be calculated for the boundary condition of an adiabatic fin tip to determine the efficiency along the fin [Chen and Chen, 2013].

$$\eta_{fin} = \frac{Tanh(ml)}{ml} \tag{4.15}$$

m is a parameter of the fin that describes the exponential temperature decrease along the fin's length and l is the effective height of the fin.

$$m = \sqrt{\frac{2H}{kw_f}} \tag{4.16}$$

$$l = \frac{H}{2} - w_f \tag{4.17}$$

Here, H is the height of the fin, k is the thermal conductivity of the material used in the fin, and w_f is the width of the fin. To know the heat transfer capabilities of a full size heat sink, many factors have to be taken into consideration, such as the temperature at the heat source T_s, the temperature at the base T_b, and the temperature from the surrounding fluid T_∞ [Hamburgen, 1986].

Figure 4.4 below shows the path of heat transfer for a heat sink. The thermal resistance in figure 4.4 can be split up into different sections according to Mills [1992]. The thermal resistance at the base plate R_b, the thermal resistance in the unfinned area $R_{unfinned}$, and the thermal resistance in the finned area R_fin are summed up as a total thermal resistance R_T.

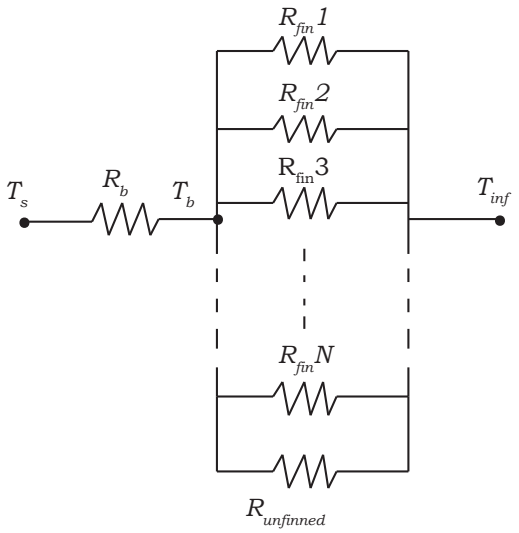

Figure 4.4: Parallel paths of heat transfer at a finned surface

The thermal resistances of the different sections can be identified through the following equations.

$$R_b = \frac{L}{kA_s} \tag{4.18}$$

$$R_{fin} = \frac{1}{\eta_{fin} h A_{s,fin}} \tag{4.19}$$

$$R_{unfinned} = \frac{1}{h\left(A_{sb} - N_{fin} A_{cb}\right)} \tag{4.20}$$

$$R_T = R_b + \left(\frac{1}{R_{fin}} + \frac{1}{R_{unfinned}}\right)^{-1} \tag{4.21}$$

L describes the length of the heat sink, W is the width of the heat sink, A_s is the area of base, h is the convective heat transfer coefficient of the coolant fluid. N_{fin} is the number of fins in the heat sink, $A_{s,fin}$ is the surface area of the fin

$(2(w_f + L)H)$, A_{sb} is the base surface area of the heat sink (WL), and A_{cb} is the cross section base area in the unit area of $(N_{fin}w_fL)$. Values for temperature in the heat sink can be solved with Eq. 4.21 by setting boundary conditions in the heat sink.

4.3 Finite volume method

The physical process of a fluid flow has to be represented as a mathematical formulation in a numerical simulation, where fundamental laws from both engineering and physics are applied in mathematical methods [Majumdar, 2005].

4.3.1 Iteration

An iterative solver in a Computational Fluid Dynamics (CFD) application is used to solve the algebraic equation in a matrix algorithm. The method of the iterative process reduces the initial residual of the simulation values through multiple iterations. The values of the simulation are updated through every iteration until the residual of the solution is sufficiently small to be considered converged. The iteration is necessary to be able to solve a nonlinear equation in the CFD algorithm. Moreover, it greatly reduces the requirements of memory to get an efficient matrix for a solution [Bhaskaran and Collins, 2002].

4.3.2 Integration over control volume

The formulation of basic laws in a finite volume method can be done with an integration in a convection-diffusion equation. The fluxes of a transport property ϕ are a part of getting a set of conservation equations in a discrete form. The transport equation for ϕ properties are written as follows.

$$\left(\frac{\partial(\rho\phi)}{\partial t}\right)_{Transient} + (div(\rho\phi u))_{Convective} = (div(\Gamma\nabla\phi)_{Diffusion} + (S_\phi)_{Source} \tag{4.22}$$

Γ is the diffusion coefficient, ρ is the density of the fluid, u is the velocity vector of the fluid, and t is the time. S_ϕ and ϕ can represent 1, T, h_0, u, v, or w [Versteeg and Malalasekera, 2007].

In Eq.4.22, the term of transient can be described as the rate of increase of ϕ of a fluid element, and the term of convection can be described as the net rate of flow of ϕ out of fluid element. The term of diffusion can be described as the rate

of increase of ϕ because of diffusion and the term of source can be described as the rate of increase of ϕ because of sources [Versteeg and Malalasekera, 2007].

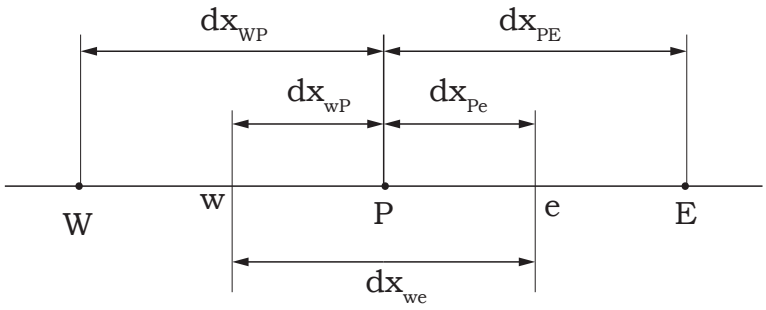

Figure 4.5: One dimensional finite volume

In figure 4.5, P is the cell containing node in a control volume, W and E are the neighbouring nodes to the west and east, respectively. The cell faced to the west and east are given a symbol of w and e, respectively. The distance between P and W is shown as dx_{WP} and the distance between P and E is shown as dx_{PE}. The distances of the volume faces w and e from nodal point P are shown as dx_{wP} and dx_{Pe}, respectively. The width of the control volume is represented as $\Delta x = dx_{we}$ [Versteeg and Malalasekera, 2007].

An integration of a one-dimensional control volume will give the following equation.

$$(\rho u A_e \phi)_e - (\rho u A_w \phi)_w = \Gamma_e A_e \left(\frac{d\phi}{dx}\right)_e - \Gamma_w A_w \left(\frac{d\phi}{dx}\right)_w \tag{4.23}$$

A is the cross sectional area of the control volume. As $A{=}A_e{=}A_w$, terms of both sides of Eq.4.23 can be divided by the area A.

4.3.3 Solution of equation

A discretization scheme is used to solve the equation for the convection-diffusion problem from the transport equation. The order of accuracy is a measurement between nodes and cell faces in the finite volume in the calculations of discretisation scheme. All discretization schemes have the same purpose, which is to set the discrete equation of each nodal point into a set of coefficients to be solved with a matrix solution technique [Versteeg and Malalasekera, 2007].

4.4 Optimization theory

The problem formulation process for an optimum design was described in literature by Arora [2004] as a tool to make sure that a system will have minimum time and money spent on it, while having the system work with highest capability. The problem formulation process [Arora, 2004] is described by the following steps.

- Project/problem description
- Data and information collection
- Definition of design variables
- Optimization criterion
- Formulation of constraints

The *project/problem description* builds the basis for the following process, in which the objective of and the requirements for the design are set.

The *data and information collection* is a process of information gathering, where for example the properties and cost of materials used in the system have to be identified. Also at this stage in the process, the analysis procedures and analysis tools have to known to be able to do an analysis of trial designs.

The *definition of design variables* includes the description of the system done with sets of variables, such as parameters. It is better if the variables are independent of each other, because dependent variables are effected by a change of other variables.

The *optimization criterion* is the step in the process to find out the best design with set variables. A function can be made to get an ideal design from a set of desired results. If the desired value is the ideal point between cost (C) and heat transfer ($\dot{Q}$), then the function can be described as $f(C, \dot{Q})$.

The *formulation of constraints* is the last part of the problem formulation process, where the constraints of the system are analysed to get realistic results. A system must be able to work under a certain load without failing. Constraints are set on working load and space that the system cannot exceed. Subsequently, an optimal system can be build within those boundaries [Arora, 2004].

Methodology

5

The methodology used for determining the optimal design in terms of thermal performance is described in this chapter (CH. 5.1), including an introduction of the design variables (CH. 5.1.1) and the operating conditions (CH. 5.1.2). The methodology used for the cost analysis, which is conducted in addition to the thermal efficiency analysis, is presented (CH. 5.2). This builds the basis for modelling the thermal distribution in the heat sink. Techniques used for modelling are presented thereafter (CH. 5.3).

5.1 Optimization method

One main objective of this study is to find the heat sink design with the lowest thermal resistance R_t. To do so, the optimization method used in previous studies of Li and Peterson [2006] was used.

5.1.1 Design variables

A number of possible heat sink designs are compared, and thus simulations are conducted with different values for the design variables. Some design variables were chosen as fixed assumptions, while others were variable and thus subject of the optimization analysis.

The design variables relevant to the heat sink design in the present study are displayed in figure 5.1 and labeled accordingly. The dimensions of the heat sink in question are defined by an area of the base plate (A), which was chosen to be fixed at 100 mm^2, with the fixed height of the channels at 0.320 mm. Moreover, the present study is focused on a heat sink that is made of aluminum and has insulation on top of it, where there is no heat transfer between the aluminum and the insulation.

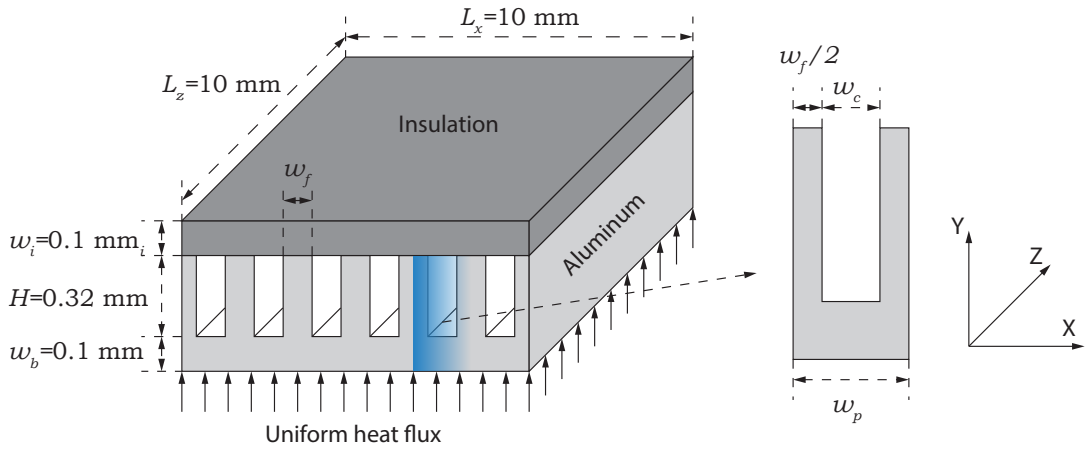

Figure 5.1: Design variables in heat sink used in this study

The bottom width w_b is fixed at 0.1 mm as it is above the minimum recommended thickness of base at 0.05 mm for a micro channel heat sink with a area of 10×10 mm [Li and Peterson, 2006].

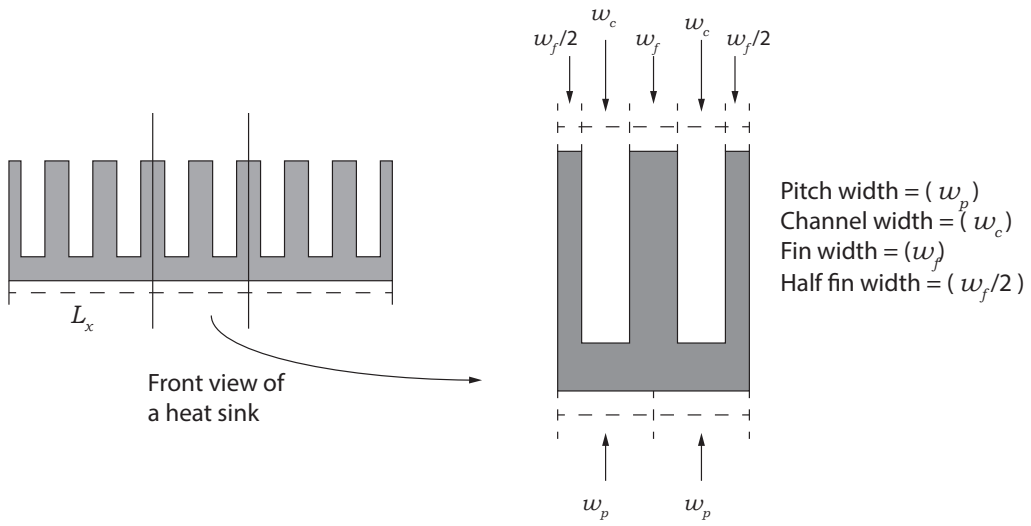

Figure 5.2: The pitch as a unit of analysis for simulation

Figure 5.2 shows a heat sink and illustrates the segment of the heat sink which is used as the unit of analysis for which simulations are conducted. This segment is referred to as a pitch. As figure 5.2 illustrates, the area of w_p is made up of the

channel width w_c and two half fin widths $w_f/2$. The pitch's width w_p is influenced by the entire width of the heat sink L_x and the number of channels N in it and can be identified with the equation $w_p{=}L_x/N$. If, for example, L_x equals 10 mm and N equals 10, the w_p will be 1 mm for the whole width of the channel. With an increasing number of channels, the pitch width decreases.

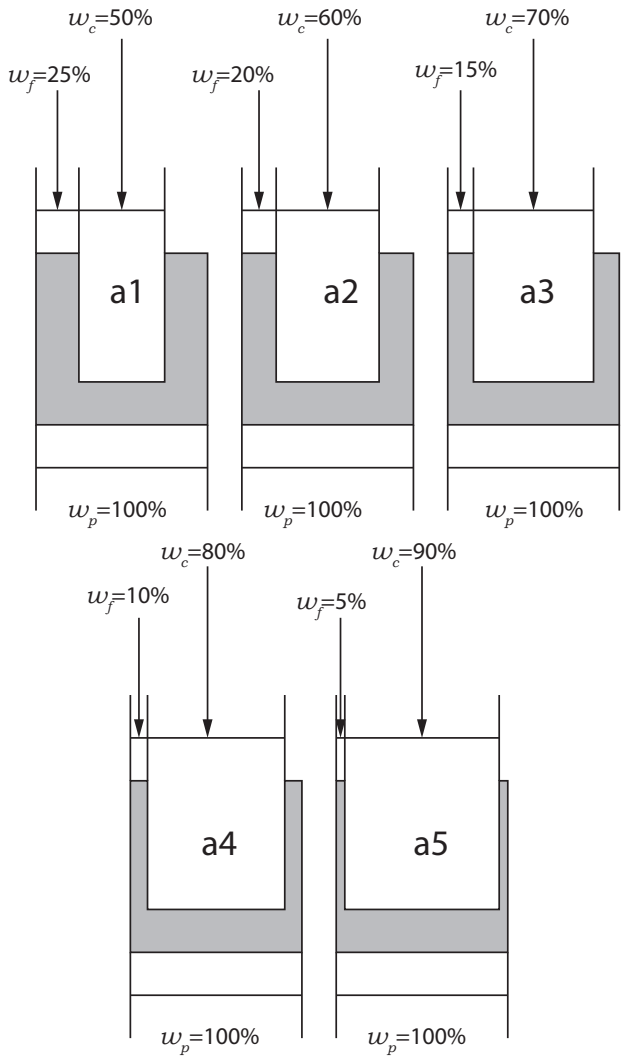

Figure 5.3: Width ratio of the channels

Heat sink designs with different ratios between channel width w_c and fin width w_f are displayed in figure 5.3. These range from a design scenario with a comparably

narrow channel and thick fins, meaning low β, in scenario a1, to a design scenario with a very wide channel and thin fins, meaning high β, in scenario a5.

Table 5.1 shows how the values for the channel width w_c and fin width w_f decrease when the heat sink has 20 instead of 10 channels (N) and the pitch of the width w_p accordingly is narrowed from 1 down to 0,5 mm. While the width ratio stays the same and displays the same ratios as indicated in fig. 5.3, the absolute values of channel and fin width decrease when the number of channels increases.

Table 5.1: Individual parameters at a fixed area of 10 × 10 mm for 10 and 20 channels

N	w_p (mm)	β	w_c (mm)	w_f (mm)	Figure 5.3
		0.5	0.5	0.5	a1
		0.6	0.6	0.4	a2
10	1	0.7	0.7	0.3	a3
		0.8	0.8	0.2	a4
		0.9	0.9	0.1	a5
		0.5	0.25	0.25	a1
		0.6	0.3	0.2	a2
20	0.5	0.7	0.35	0.15	a3
		0.8	0.4	0.1	a4
		0.9	0.45	0.05	a5

Table 5.2 summarizes the values selected for the design variables used.

Table 5.2: Design variables of the micro channel heat sink

Description	Values
Channel length (L_z)	10 mm
Base plate width (L_x)	10 mm
Insulation width (w_i)	0.1 mm
Channel and fin height (H)	0.32 mm
Bottom thickness (w_b)	0.1 mm
Fin width (w_f)	0.01 - 0.5 mm
Channel width (w_c)	0.05 - 0.9 mm
Width of pitch (w_p)	1 - 0.1 mm
Number of Channels (N)	10, 20, 30 100
Width ratio (β)	0.5, 0.6, 0.7, 0.8, and 0.9

The main simulations in this study are performed with different values for the design variables at 10, 20, 30, 40, 50, 60, 70, 80, 90, and 100 channels in a heat sink

at fixed area of 10 × 10 mm. With the height of the channels H is fixed 0.32 mm, with a width ratio β of 0.5, 0.6, 0.7, 0.8, and 0.9 for every number of channels in the heat sink.

Additionally, the designs at the channel height of 0.32 mm, will be compared to designs for the same number of channels N and width ratio β at a channel height of 0.64 mm and 0.96 mm for the same fixed area of heat sink, to see how much the height of the channel can influence the thermal distribution.

5.1.2 Operating conditions

The values of thermal resistance will be used to compare the thermal capabilities of every design of heat sink in this study. This has been also done in a previous study by Li and Peterson [2006] that compared heat sinks with differently sized channels. An equation from previous work by Husain and Kim [2008] is used in this study to compare the thermal resistance in heat sinks with channels of different sizes.

$$R_t = \frac{T_{solid} - T_{fluid}}{\dot{q}} \tag{5.1}$$

The equation indicates that several values are necessary to determine the thermal resistance (R_t) in the channel of a heat sink, namely the temperature of the fluid (T_{fluid}) and the solid (T_{solid}) is needed, as well as the heat flux coming into the channel ($\dot{q}$). These relate to the conditions the heat sink is operating in. Just like design variables, some of the operating conditions have been set as fix for the analysis in the present paper, while others have been variable and thus tested in the simulations.

5.1.2.1 Heat flux uniformity and temperature

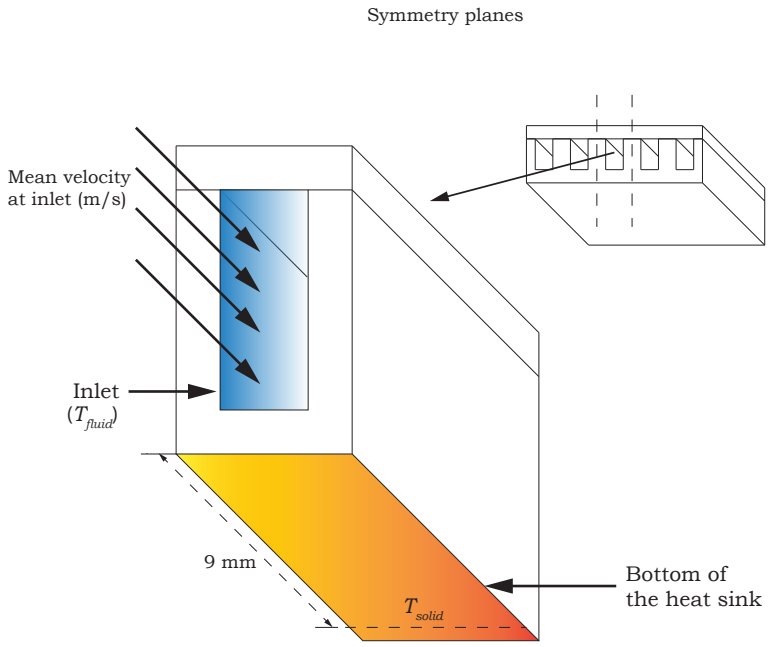

Figure 5.4: Location in a heat sink design for which a certain temperature is assumed

The temperature values are set for locations that are indicated in figure 5.4. T_{solid} describes the temperature at the bottom of a heat sink, 9 mm away from the inlet and thus 1 mm away from the outlet. T_{fluid} is the temperature of the fluid coming into the inlet.

The method of the previous study by Husain and Kim [2008] is used to determine the thermal resistance. $\dot{q}$ is chosen to be 250 kW/m^2, 500 kW/m^2, and 750 kW/m^2 to compare and see if the thermal resistance is independent of changes in the heat fluxes. The $\dot{q}$ in Eq. 5.1 will be represented as 25 W/cm^2, 50 W/cm^2, and 75 W/cm^2. T_{fluid} is chosen to be 300 K. The value for the temperature was chosen from previous studies, were this temperature is very common as an initial temperature in a cooling system [Tuckerman and Pease, 1981].

T_{solid} is the only variable in the equation 5.1 that is varying between the simulated designs. The simulations thus indicate how different designs of heat sinks influence the temperature of the solid in the specified location. A higher T_{solid} means a higher thermal resistance R_t and thus a worse thermal performance of a heat sink design.

5.1.2.2 Pumping power as a fixed variable

This study could have been focused on the fluid flow into the channel at a fixed velocity for all heat sink designs or, alternatively, at a fixed pressure loss along the length of the heat sinks L_z. However, the pumping power $\overline{P}$ was chosen as a fixed variable to find the optimum design of a heat sink as it has been used in previous studies [Li and Peterson, 2006]. Using a fixed pumping power for all designs will give more useful results of optimisation, as fixed velocity and pressure loss would lead to varying amounts of energy used for the pumping power. A higher energy use would most likely also not be in the sense of optimization. To find the $\overline{P}$ for a rectangular channel in a heat sink, the following equation is used [Li and Peterson, 2006].

$$\overline{P} = \dot{V} \cdot \Delta P = N \cdot v_{mean} \cdot H \cdot w_c \cdot \Delta P \tag{5.2}$$

$\dot{V}$ is the volumetric flow (m^3/s) and ΔP is the pressure loss along the channel (Pa). The pumping power is given as a function of $\dot{V}$ and ΔP, where $\dot{V}$ is defined by the number of channels N, the mean velocity of the fluid v_{mean}, and the height H and the width w_c of the fin [Li and Peterson, 2006]. To be able to conduct the simulations at a fixed $\overline{P}$, v_{mean} has to be calculated for every aspect ratio α of the channels. The formulation of the mean velocity v_{mean} in relation to the pumping power is outlined in the following steps.

The Reynolds number Re in relation with the v_{mean} is described as

$$Re_D = \frac{\rho v D_h}{\mu} \tag{5.3}$$

where ρ is the fluid density and μ is the dynamic viscosity.

The hydraulic diameter (D_h) in the channels is defined by the following equation.

$$D_h = \frac{4ab}{2(a+b)} \tag{5.4}$$

a is the vertical length and b is the horizontal width of the channel [Husain and Kim, 2008].

The friction factor (f) can be formulated by rearranging the pressure loss equation (equation 4.10 in CH. 4.2.4) to give the following equation.

$$f = \frac{D_h}{2\rho v_{mean}^2} \frac{\Delta P}{L_z} \tag{5.5}$$

However, the friction factor f in a laminar flow can also be described as a function of the Reynolds number in a rectangular channel in a set of equations from a previous study by Knight et al. [1992a].

$$f = \frac{\gamma}{Re} \tag{5.6}$$

Using this equation is preferable as it can be incorporated in the equation to determine v_{mean} (see equation 5.10 below). In Knight's equation, the channels' aspect ratio α determines γ. For these calculations, the value of γ is determined by the equation

$$\gamma = 4.70 + 19.64G \tag{5.7}$$

in which the value of a straight lines least square fit in G are put in Eq. 5.7 [Knight et al., 1992a].

$$G = \frac{H^2 + {w_c}^2}{(H + w_c)^2} = \frac{\alpha^2 + 1}{(\alpha + 1)^2} \tag{5.8}$$

The values gathered from the Eq. 5.6-5.8 are within $\pm 3\%$ of the except value in literature from Kays and Crawford [1993] according to a study by Li and Peterson [2006].

The mean velocity in the channel can be determined from Eq. 5.6 by substituting the values Re and f, with other values from Eq. 5.3 and 5.5, respectively. Leading to the following equation,

$$v_{mean} = \frac{D_h^2}{2\gamma\mu} \frac{\Delta P}{L} \tag{5.9}$$

The value of ΔP is a function of v_{mean} and not v_{mean}^2 due to the influence of the Re in Eq. 5.9. The values in Eq. 5.2 can be substituted into Eq. 5.9 for the ΔP, to give the following equation.

$$v_{mean} = \sqrt{\frac{D_h^2}{2\gamma\mu}\frac{1}{L_x}\frac{1}{Nw_fH}\overline{P}} = \sqrt{\frac{2}{\gamma\mu}\frac{\alpha}{(\alpha+1)^2}\frac{1}{NL}\overline{P}} \tag{5.10}$$

The value of v_{mean} can be found for every number and design of channel in a heat sink with a fixed $\overline{P}$ [Husain and Kim, 2008].

The fixed pumping power will be set at 0.01 W, as the difference in size of the cross sectional areas at 10 channels to 100 channels is big. Setting a fixed pumping power at a small rate will guarantee that the flow regime of all the channels in this study will be considered a laminar flow, as the Reynolds number is considered to be at critical values from 1900 to 2800 depending on the aspect ratio of the channel [Hanks and Ruo, 1966].

5.1.2.3 Source of the uniform heat flux

The heat flux coming into the heat sink can have different sources. In the present study, it was chosen to derive from a Insulated Gate Bipolar Transistor ($IGBT$) "FGH40N60UFD" [Fairchild Semiconductor Corporation, 2008], which is a semiconductor that has four alternating layers (P-N-P-N) that are controlled by a metal-oxide-semiconductor gate. It can by used in multiple applications such as electric cars, microwaves, air conditioners, and solar inverter. It is assumed that there is no thermal resistance between the heat sink and the $IGBT$, as discussed in the previous chapter (see 4.1.3). Real applications would always have some contact resistance and depending on the application there could be material such as base plate or copper spread plate that would have some thermal resistance.

To summarize, the operating conditions used in this study for the optimisation of the micro channel heat sink are listed in table 5.3.

Table 5.3: Operating conditions of the micro channel heat sink

Description	Values
Pumping power ($\overline{P}$)	0.01W
Temperature of fluid at inlet (T)	300 K
Uniform heat flux ($\dot{q}$)	250 kW/ m^2, 500 kW/ m^2, and 750 kW/ m^2

5.2 Cost analysis method

The optimization of cost and thermal performances was conducted by combining results from CFD and costs from heat sink manufacturer Micro Logic Corporation [2004]. By having the performance results from numerous designs of heat sinks in the CFD, a method of optimization was conducted in *Matlab* to determine the optimum design of a heat sink by combining the cost function and thermal performance of each individual design of heat sink.

The cost (C) of a customized rectangular heat sink was gathered from emachineshop [Micro Logic Corporation, 2004]. The cost of each cut for a channel in a heat sink was acquired, in order to develop a cost function with increasing number of channels on a fixed area of heat sink at 10 $\times$ 10 mm.

The cost and the thermal capability are essential in choosing the ideal material for a heat sink. The most popular materials for the heat sink are copper (385 W/mK) and aluminum (205 W/mK) [Powell et al., 1966] even though materials such as silver and diamond have higher thermal conductivity k, around 400 and 1000 W/mK, respectively [Powell et al., 1966]. This is because aluminium and copper as base metals with costs at 2.03 \$/kg and 7.15 \$/kg (as of April 2019) [Euromoney Institutional Investor PLC, 2019], respectively, are much cheaper compared to these precious metals. Copper has higher thermal conductivity than aluminium, but aluminium is an ideal alternative for a cheaper designs and also a much lighter component [Powell et al., 1966].

Not only the material choice has impact on the costs, but also the design of the heat sink. This study focuses on the design part by using a cost function that describes manufacturing costs of a heat sink in relation to the cuts of the fins

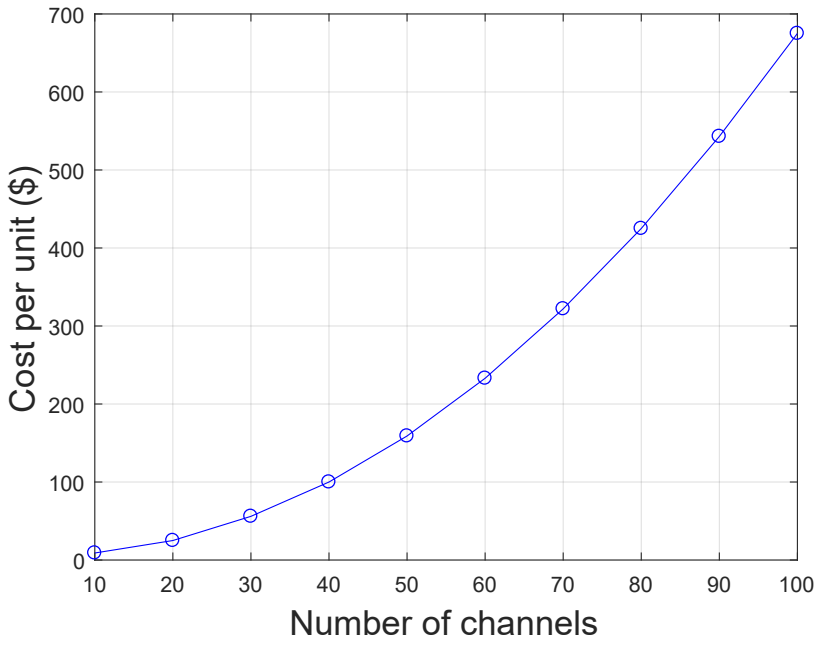

Figure 5.5: cost of a heat sink in relation to the amount of channels [Micro Logic Corporation, 2004]

Figure 5.5 indicates that the cost of a micro channel heat sink rises with each cut in the manufacturing process,

Table 5.4: Costs of the heat sink in relation to different amounts of channels [Micro Logic Corporation, 2004]

N	5	10	20	30	40	50	60	70	80	90	100
Cost per unit $	7	9	25	56	100	159	233	322	425	543	675

The costs rises higher at each step size of 10 channels, and the difference in cost is highest between 90 and 100 channels at 132 $. The cost set by the selected manufacturer is dependent on the quantity of heat sink units purchased. In this study, an exemplary amount of 10 units was chosen. While heat sinks with few channels are common, heat sinks with more channels are not, and therefor require customized manufacturing. This customization, but also a more complex manufacturing process, explains the rise in costs with an increasing number of channels (see fig. 5.5). By choosing an exemplary purchasing amount of 10 units, the present analysis provides an indication of the relationship between costs and thermal per-

formance. However, an interpretation of the results should take into consideration that customers which request heat sinks with a high number of channels might order a bigger number of units and thus keep costs lower than indicated here.

The optimal design of the cost and thermal distribution will afterwards be used in a simulation at a transient behavior of heat flux $\dot{q}$, for an analysis at more realistic set up then in the previous simulations at steady state. The variation of temperature in a heat sink design will be analysed under different operating conditions, to see if the highest temperature in the design will exceed maximum operating temperature of the IGBT.

5.3 Modelling Methodology

5.3.1 Software Choice

Software by the provider ANSYS for computational fluid dynamics (CFD) was used to analyze and answer problems that involve fluid flows, by using data structures and fluid mechanics [Stolarski et al., 2018]. By using CFD software for the analysis of a fluid flow, instead of experimenting on a component in a laboratory, a large amount of cost and time can be minimized. Also, the CFD can give relatively precise results close to real life experiments [Toh et al., 2002]. Before making a simulation in CFD, a few steps had to be followed to get realistic and reliable results. The geometry and design of the heat sink for the simulation was created using the design software solidworks [Lombard, 2008]. The design file could subsequently be imported to ANSYS' software Icem, which is an extension of ANSYS CFD. It was used to create the physical bounds and to create a mesh, which allows to break down the larger structure of the heat sink area into small components. With the structure of the simulation in place, the boundary conditions and simulations were done in ANSYS *Fluent*. For an eased work process involving these softwares, ANSYS' software environment *workbench* was used. After the completed simulation, the post processor analysis in ANSYS workbench created a visualization of the result [Anderson and Wendt, 1995].

5.3.2 Assumptions and simplifications for the physical model

1 The Laminar flow is assumed to be in-compressible.
2 Thermophysical properties of the solid are assumed to be constant.
3 Radiation, viscous heating, and gravitational effects are negligible
4 Hydraulically and Thermally fully developed flow is assumed.

5.3.3 Properties of fluid and solid

Water is used as a coolant in this project, where the fluid properties are in this study assumed to be constant over the temperature range. The thermophysical properties in this project are listed in table 5.5.

Materials	ρ (kg/ m ^{3})	c_p (J/kg· K)	k (W/m· K)	μ (kg/m· s)
Deionized water	997	4180	0.607	0.000891
Aluminum	2719	871	205	-

Table 5.5: Thermophysical properties of the coolant and solid, T= 300 K [Powell et al., 1966]

ρ is the density, c_p is the specific heat, and μ is the dynamic viscosity.

5.3.4 Governing equations

Based on the assumptions in CH. 5.3.2 , the governing equations for the numerical model are as follows:

The continuity equation:

$$\nabla \cdot (\rho_f \vec{V}) = \quad 0 \tag{5.11}$$

ρ_f is the fluid density and $\vec{V}$ is the velocity vector with u, v and w as velocity components in direction of x, y and z, respectively.

The momentum equation for fluid:

$$\vec{V} \cdot \nabla(\rho_f \vec{V}) \quad = -\nabla p + \nabla(\mu_f \nabla \vec{V}) \tag{5.12}$$

μ_f is the dynamic viscosity of the fluid and p is fluid pressure.

The energy equation for the fluid:

$$\vec{V} \cdot \nabla(\rho c_{p,f} T) = \nabla \cdot (k \nabla T_f) + \dot{q} \tag{5.13}$$

$c_{p,f}$ is the fluid heat capacity, T_f is the temperature of the fluid, k_f is the thermal conductivity of the fluid and $\dot{q}$ is the uniform heat flux coming into the heat sink.

The energy equation for the solid region:

$$\nabla \cdot (k_s \nabla T_s) + \dot{q} = \quad 0 \tag{5.14}$$

k_s is the thermal conductivity of the solid and T_s is the temperature of the solid.

The energy equation for fluid in a transient state:

$$\rho c_p \frac{\partial T_f}{\partial t} + \vec{V} \cdot \nabla(\rho C_{p,f} T) = \nabla \cdot (k \nabla T_f) + \dot{q} \tag{5.15}$$

The energy equation for solid region in a transient state:

$$\rho c_p \frac{\partial T_s}{\partial t} = \nabla \cdot (k_s \nabla T_s) + \dot{q} \tag{5.16}$$

5.3.5 Boundary Conditions

The boundary condition of the micro channel heat sink are as followed: Inlet (velocity inlet):

$$u = u_{in}, v = 0, w = 0 \quad and \quad T = T_{in} \tag{5.17}$$

Outlet (pressure outlet):

$$p = p_{out} \tag{5.18}$$

Interface of fluid-solid:

$$u = 0, v = 0, w = 0 \quad and \quad T = T_{in} \tag{5.19}$$

The heat flow wall:

$$q_w = -k_s \frac{\partial T_s}{\partial n} \tag{5.20}$$

For other solid walls and symmetric boundaries:

$$-k_s \frac{\partial T_s}{\partial n} = 0 \tag{5.21}$$

5.3.6 Numerical method

The Navier Stokes equations are solved using the finite volume method (FVM) in CFD commercial package (ANSYS FLUENT).

The combined convection-diffusion effects in the transport equation were modeled by the second order upwind scheme and the pressure-velocity coupling is solved by using the SIMPLE algorithm. The TDMA (tri-diagonal matrix algorithm) line-by-line was used for the algebraic equations. The solution in the simulation was

considered to be converged at 10^{-6} for continuity equation and the energy equation was considered to be converged at 10^{-9}.

One channel in the heat sink was simulated in this study, composed of one channel width w_c and two half fin widths w_f with a symmetry at the outer surface on both side of the half fins.

By performing the simulation with a symmetry plane at one channel, computational time and resources are minimized [Zhou et al., 2016; Ermagan and Rafee, 2018; Karathanassis et al., 2013]. The boundary conditions of all channels are assumed to be the same, as natural heat exchange between surrounding air and the surface of the fins is neglected as being adiabatic at the outer surface of the heat sink [Xianghui and Feng, 2011].

5.3.7 Grid independency study

The study of grid dependency is a really important tool to evaluate the optimum grid size of a simulation. The aim is to compare a coarse grid to a finer grid and see if the results of the coarser grid is compromised [Roache, 1998].

A very fine grid can take up a lot of finite computing resource and time, which can lead to a large computational expense. By using a coarser grid that will not compromise the result and will require much less computational expenses, an optimum size of a mesh can be obtained [Roache et al., 1986].

Different methods have been used to find the most accurate estimation of the discretization error. A widely recommended method to use is the Richardson extrapolation method. It is the most widely studied and reliable method available [Celik et al., 2008]. A method often used to determine the ordered discretization error is the Grid Convergence Index (GCI), which is based upon the theory of Richardson extrapolation method. The (GCI) is a method of estimating the grid refinement error, by examining the simulations spatial convergence [Roache, 1998].

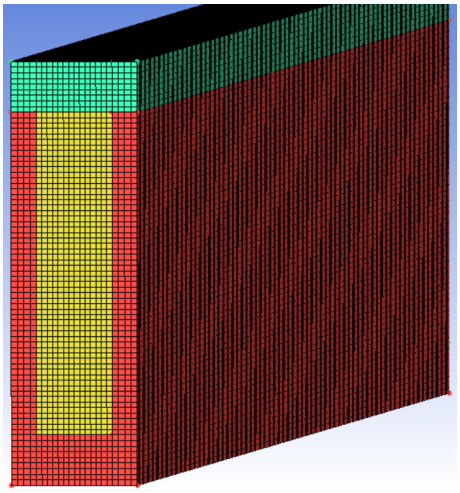

Figure 5.6: Grid size of 25(x)×70(y)×450(z)

The method of declaring the grid independency of a simulation in this study will be following the steps used in a study from Celik et al. [2008], which can be seen in more details in the **Appendix**.

The three different grid sizes are chosen in this study for the estimation of the discretization error for a chosen channel size of H=0.640 mm, w_c=0.15 mm, and w_c=0.05 mm. The size of grid used in the simulation of the channel is 25(x)×70(y)×450(z). It was compared to the finer grid sizes of 30(x)×100(y)×500(z) and coarser grid size of 20(x)×50(y)×400(z). The parameter used as a variable for declaring the grid size dependency in this study is pressure loss in a channel.

Table 5.6: Reference grid, fine grid, and coarse

	Number of cells	Pressure loss (Pa)
Reference grid size	787.500	4869
Fine grid	1.500.000	5014
Coarse grid	400.000	4685

The values in table 5.6 were used to estimate the discretization error for the different grid sizes.

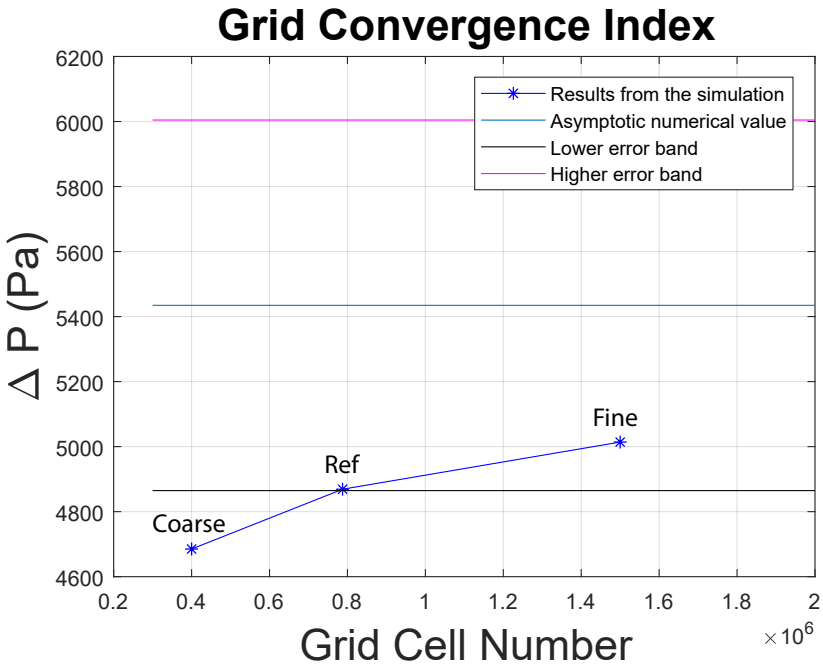

Figure 5.7: Grid Convergence index

As can be seen in figure 7.2, two of the grid sizes converge within the error band of the asymptotic numerical value. As two of the grid sizes are within the error band, the size with the least amount of cells is the most suitable to use.

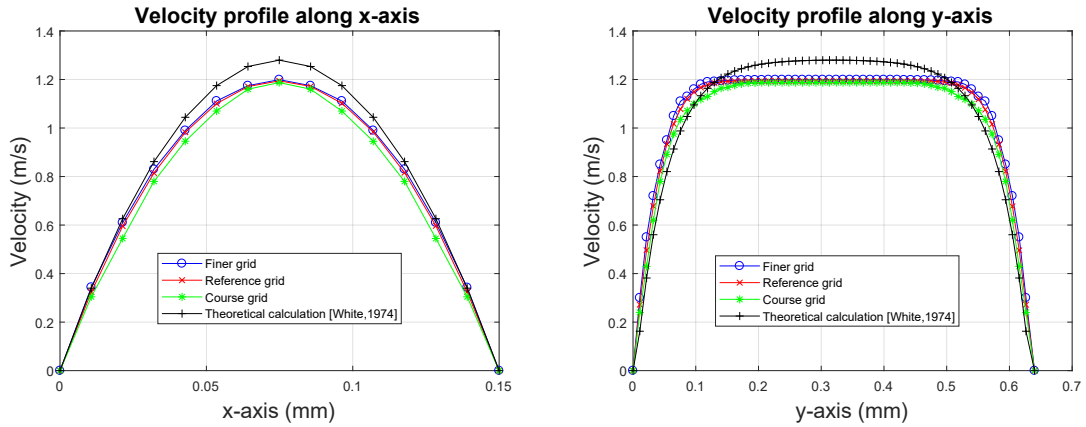

(a) Velocity profile on x-axis **(b)** Velocity profile on y-axis

Figure 5.8a shows a velocity profile at a centerline at x-axis in the middle of the channels height in y-direction in a fully developed flow for all three different

grid sizes used in the (GCI) and theoretical calculations from White [1974] for comparison. The highest velocity at the centerline is 1.1944 m/s for the reference case, 1.1993 m/s for the finer grid and 1.1872 m/s for the coarser grid at a mean velocity of 0.7258 m/s coming into the channel. Figure 5.8b shows the velocity profile of the same grid sizes at y-axis in the channel, where a cross cut of the y-axis area is taken in the middle of the channel in x-direction in a fully developed flow.

The mesh generated for all simulations in this study is composed by a orthogonal-full-hexahedral mesh, with aspect ratio of ~ 1 and zero skewness, ensuring a very good quality mesh.

The size of a cell in x and y direction at a grid size of 25(x)×70(y)×450(z) at H=0.640 mm, w_c=0.15 mm and w_c=0.05 mm is Δx of 0.0107 mm and Δy of 0.0108 mm. The size of channels will vary in this study, while the size of a cell will be fixed, with larger or smaller number smaller number of cells used for different simulations.

5.3.8 Verification of the numerical code

Three different channels in a heat sink were simulated and compared to existing results from these specific channels in a experimental case from Tuckerman and Pease [1981] and numerical case of Toh et al. [2002] for a verification of the numerical code used in this study. The R_t in the channels was used to compare the results from the current simulation, to the existing ones. All three designs were for 100 channels in a heat sink for an area of 10 × 10 mm cold plate of silicon substrate, which has the density ρ of 2330 kg/m^3, specific heat c_p of 703 W/kgK and the thermal conductivity of 148 W/mK for a temperature of 300 K [elements].

Table 5.7: Comparison of thermal resistance between experimental and computational results

Interface	Channel 1	Channel 2	Channel 3
w_c (mm)	0.056	0.055	0.05
w_f (mm)	0.044	0.045	0.05
H (mm)	0.32	0.287	0.302
Heat flux (W/cm^2)	181	277	790
Fluid flow (liters/minute)	0.282	0.39	0.516
R_t (K/W) [Tuckerman and Pease, 1981]	0.110	0.113	0.09
R_t (K/W) [Toh et al., 2002]	0.157	0.128	0.105
R_t (K/W) Current study	**0.149**	**0.120**	**0.104**

Results from the CFD simulation in this study gave an error of 35.5 % in channel 1, 6.2 % in channel 2 and 15.6 % in channel 3 of the thermal resistance of from the experimental study of Tuckerman and Pease [1981] in Table 7.1.

Additionally, the results from the CFD simulation in this study gave an error of 5 % in channel 1, 6.25 % in channel 2 and 0.9 % in channel 3 of the thermal resistance of from the numerical study of Toh et al. [2002].

Results

6

This chapter presents the results of the optimisation method outlined in CH. 5. This includes the results from the main analysis (CH.6.1) and the development of the cost compared to the designs thermal resistance (CH. 6.2). The effectiveness of an increasing fin height of 0.64 and 0.96 mm were compared to the fin height of 0,32 mm (CH.6.3) and finally the chosen optimal design was simulated in a transient state (CH. 6.4).

6.1 Thermal resistance of the heat sink designs

The thermal resistance represented the key indicator for determining the optimal heat sink design. Figure 6.1 shows the thermal resistance for designs with 10 to 100 channels at width ratios ranging from 0.5 to 0.9. Fixed parameters were an area of 10×10 mm and a channel height of 0.32 mm at a fixed pumping power of 0.01 W. The heat flux coming into the heat sink was at 500 kW/m^2 in all scenarios.

It becomes clear that thermal resistance R_t decreases with a rising number of channels in the heat sink. The thermal resistance has the biggest decrease between 10 and 20 channels at a difference of up to 28.7 %. The difference in thermal resistance becomes smaller as the number of channels becomes higher. The designs with width ratios from 0.7 to 0.9 show decreasing thermal resistance until a channel number of 80, after which it remains steady for β of 0.9 and increases in cases of β of 0.7 and 0.8. For the designs with β of 0.5 and 0.6 the thermal resistance decreases until N equals 50 and 60, respectively, before thermal resistance starts increasing again.

These simulations clearly show that a higher number of channels in a heat sink does not necessarily equal a higher thermal performance. In all cases, the thermal performance improves only up to a certain threshold, before performance stagnates or worsens.

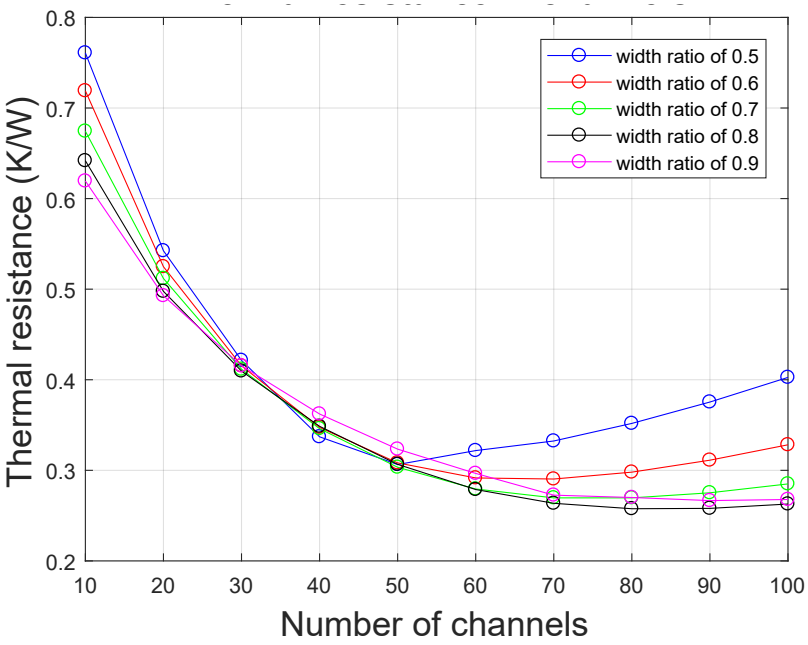

Figure 6.1: Thermal resistance in micro channel heat sinks for different designs of channels

On the basis of this analysis, an optimal width ratio β could be determined according to the amount of channels incorporated in a heat sink design. Table 6.1 shows the β for each of the ten designs with different fixed values for N (ranging from 10 to 100), which gives the lowest thermal resistance.

Table 6.1: Results from the lowest thermal resistance for each each individual channel number

N	β	$\Delta\ P$ (Pa)	D_h (mm)	v_{mean} (m/s)	Re	R_t (K/W)
10	0.9	4372	0.472	1.7021	1040	0.6194
20	0.9	4600	0.374	1.4340	670	0.4928
30	0.8	5275	0.290	1.1911	433	0.4096
40	0.5	9435	0.180	0.8783	197	0.3370
50	0.7	7351	0.195	0.8138	198	0.3034
60	0.8	7076	0.179	0.7319	171	0.2788
70	0.8	7801	0.168	0.6443	136	0.2636
80	**0.8**	**8660**	**0.152**	**0.5746**	**109**	**0.2576**
90	0.8	9486	0.139	0.5180	90	0.258
100	0.8	10208	0.128	0.4713	75	0.2628

Comparing the best case scenarios for the ten designs, the thermal resistance is lowest for the design with 80 channels and a width ratio of 0.8, where the width of the channel w_c is 0.1 mm and the width of the fin w_f is 0.025 mm. The aspect ratio α of this channel is 3.2 at a width pitch w_p of 0.125 mm.

Having determined the optimal width ratio for designs with different amounts of channels, the question arises whether these optimal width ratios are dependent on the heat flux and specific to the heat flux value of 500 kW/m^2. This is why additional simulations were conducted with heat fluxes of 250 kW/m^2 and 750 kW/m^2 for the 50 designs with different fixed numbers of channels (10-100) and width ratios (0.5-0.9). The $\overline{P}$ remained fixed at 0.01 W.

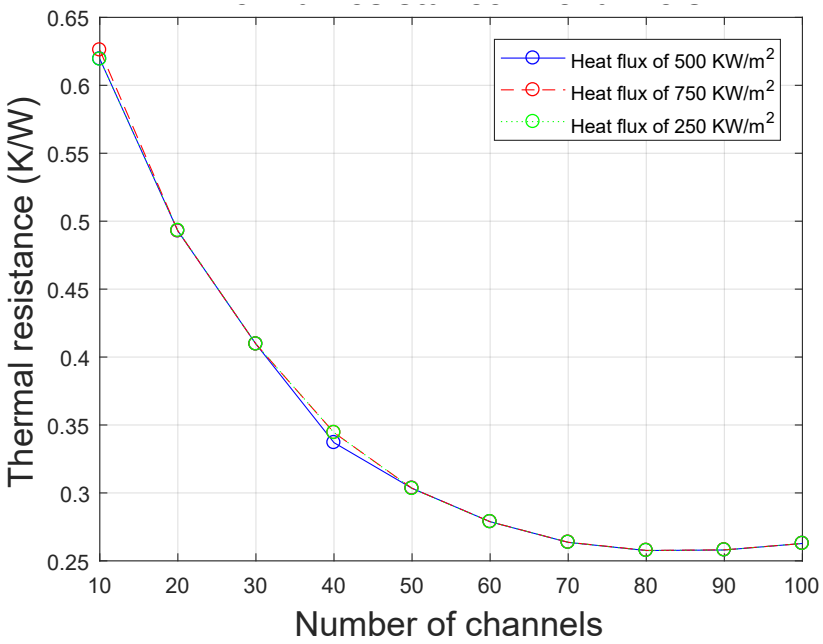

Figure 6.2: Thermal resistance in channels at different heat fluxes

The simulations resulted in an unchanged optimum width ratio for each of the ten designs. Thus, figure 6.2 shows the same ten optimal designs as previously, with heat fluxes of 250 kW/m^2, 500 kW/m^2, and 750 kW/m^2. The thermal resistance was shown to be independent of different heat fluxes coming into the heat sink.

6.2 Comparing thermal resistance and purchasing cost

The resulting designs from CH. 6.1 were put into the economical context by linking them to the purchasing cost from a selected heat sink manufacturer.

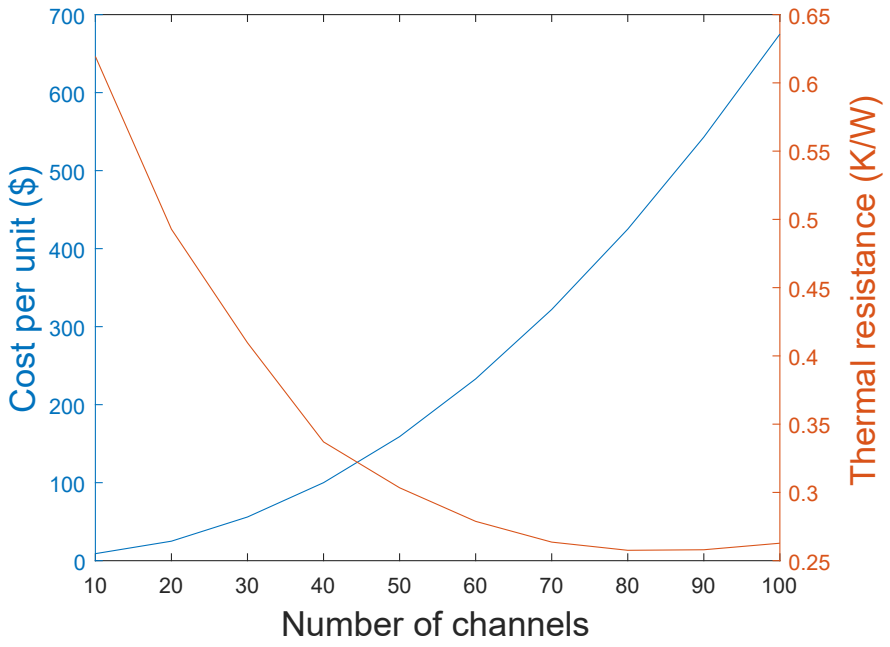

Figure 6.3: Comparison of thermal resistance and cost from manufacturer at normalized scale

Figure 6.3 shows both the thermal resistance and purchasing cost of the ten selected heat sink designs (see table 6.1). Following the designs from few channels to the ones with many channels, the decrease in thermal resistance becomes increasingly negligible, while the costs rise steeply.

Table 6.2 shows the ten selected designs, their thermal resistance, and the percentage in which the designs with more channels perform compared to the basic design of 10 channels. This value is indicated in the column labelled *Diff.10*. The column labeled *Diff.step* next to it, indicates the change in thermal performance compared to the design in the previous row. The values indicated in these two columns reflect in principle the results generated previously and show how the design with 80 channels performs best and how the design with 90 and 100 per-

Table 6.2: Difference of thermal resistance and cost between number of channels from figure 6.3. (See explanation in the following text)

N	β	R_t (Kcm^2/W)	Diff.10 %	Diff.step %	Cost $	Diff.10 %	Diff.step %
10	0.9	0.6194	-	-	9	-	-
20	0.9	0.4928	20.4	20.4	25	177	177
30	0.8	0.4096	33.87	16.88	56	522	124
40	0.5	0.3370	45.59	17.7	100	1011	78
50	0.7	0.3034	51.02	9.9	159	1666	59
60	0.8	0.2788	54.99	8.1	233	2488	46
70	0.8	0.2636	57.44	5.5	322	3477	38
80	0.8	8660	58.41	2.2	425	4622	31
90	0.8	9486	58.35	-0.15	543	5933	27
100	0.8	10208	57.57	-1.82	675	7400	24

form worse, despite higher amounts of channels. It also illustrates how the biggest increase in thermal performance is achieved in the channels with 20, 30, and 40 channels, compared to their respective precursor. The new perspective is added in the following columns, labelled Cost C, *Diff.10*, and *Diff.step*. Cost C shows the actual cost of the respective design. *Diff.10* shows the rise in cost of each design compared to the first design with 10 channels in percentage terms. *Diff.step* shows, also in percentage terms, the rise in cost for each design compared to the one in the previous row. Also here we can see that the costs for the designs with 20 and 30 channels show a sharp increase compared to the ones mentioned before in the table. While the costs rise less sharp for the designs with the higher amounts of channels, they still show an increase resulting in a cost of the design with 100 channels that is 7500% of the design with 10 channels.

The optimal design with respect to the thermal performance and purchasing cost was determined with a method from Chazelle and Edelsbrunner [1992], with which an optimal point can be found at the intersection between two variables in a plane. Figure 6.3 shows the intersection between the two variables at a point between 40 and 50 channels. The difference in thermal resistance R_t between these two parameters is at 9.9 %. By putting more emphasis on the thermal performance of the heat sink design, the optimal point is chosen to be at 50 channels.

The lowest thermal resistance at 50 channels in the heat sink was at β of 0.7 for a R_t of 0.3034 K/W. The parameters of the design are as follows, H = 0.32 mm, w_c=0.14, w_f=0.06 mm and w_p=0.2 mm.

6.3 Thermal resistance at different channel heights

The importance of the fins in the heat sink can be measured by its effectiveness at different widths and heights. The current analysis of the heat sink designs has been done at the channel height of 0.32 mm. By comparing the current analysis with designs of higher channels at the same fixed area (A) of heat sink, it can be determined if the thermal performance the heat sink would benefit from higher channels.

The heights of the channel chosen to compare with the current analysis were at 0.64 and 0.96 mm, as they were higher then the current analysis by a factor of 2 and 3, respectively.

All the designs had the same heat sink area (A) and followed the method described in CH. 5.1.

Table 6.3: Thermal resistance at channel heights H of 0.64 mm and 0.96 mm

H (mm)	N	β	ΔP (Pa)	D_h (mm)	v_{mean} (m/s)	R_e	R_t (K/W)
	40	0.6	4869	0.243	0.726	220	0.2222
	50	0.6	5742	0.202	0.590	149	0.2024
	60	0.7	5425	0.197	0.497	122	0.1920
0.640	**70**	**0.7**	**6143**	**0.172**	**0.460**	**99**	**0.1916**
	80	0.7	6920	0.153	0.405	77	0.1956
	90	0.8	6349	0.156	0.384	75	0.2004
	100	0.8	6874	0.142	0.347	61	0.2062
	40	0.5	4811	0.221	0.560	154	0.182
	50	0.6	4545	0.213	0.491	131	0.1714
	60	**0.7**	**4304**	**0.208**	**0.443**	**115**	**0.1712**
0.960	70	0.7	4900	0.181	0.381	86	0.1726
	80	0.7	5539	0.175	0.335	67	0.1778
	90	0.7	6108	0.155	0.298	53	0.185
	100	0.7	6689	0.140	0.269	44	0.1936

Table 6.3 shows the the optimal β for seven different designs with N from 40 to 100 for a channel height H of 640 and 960 mm. There is a fixed area of 10 $\times$ 10 mm and a pumping power of 0.01 W at a $\dot{q}$ of 500 kW/m^2. The lowest thermal resistance at a channel height of 640 mm is at the width ratio β of 0.7 at 70 channels and the lowest thermal resistance at a channel height of 960 mm is at the width ratio β of 0.7 at 60 channels.

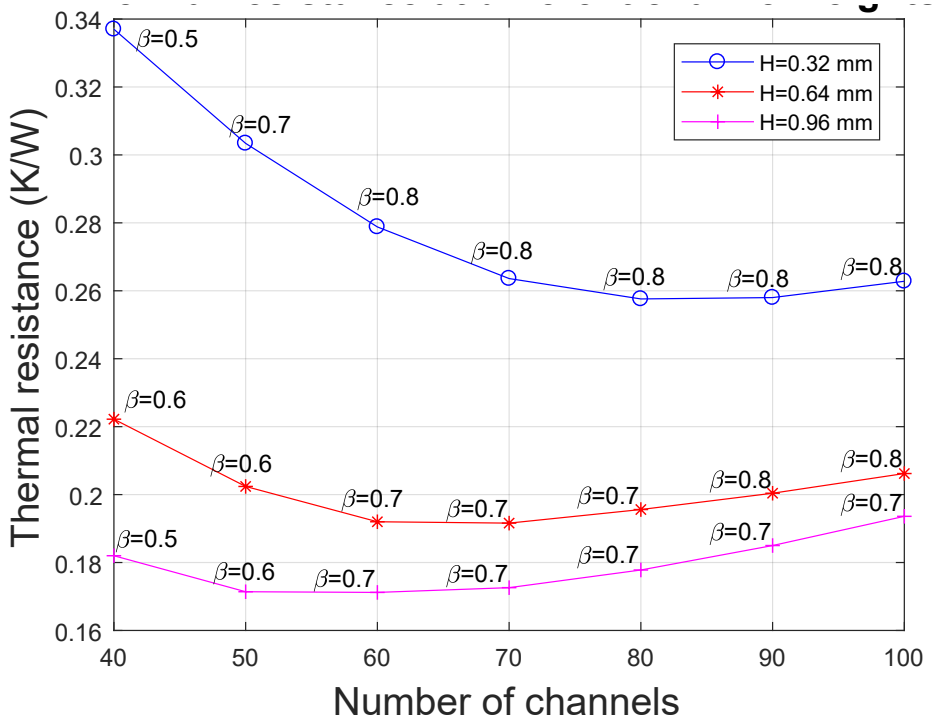

Figure 6.4: Thermal resistance at different channel height in a heat sink

Figure 6.4 shows the thermal resistance for the seven selected designs at the three different channel heights, including the channel height of 0.640 and 0.960 mm (Table 6.3) and the previously used H of 0.320 (Table 6.1). The figure shows that lower R_t in a channel at the same area of heat sink can be achieved with higher fins. The minimum thermal resistance R_t at H=0.64 and H=0.96 mm are 25.6 % and 33.5 % lower then at H=0.32 mm, respectively.

The R_t decreases for the designs with few channels but increases/stabilizes at a certain threshold between 60 and 80 channels. It can be seen that there is a strong correlation between the height of a channel and the thermal performance, with the lowest thermal resistance at the highest channel.

6.4 Heat flux at a transient state

Previous results have all been based on a steady state uniform heat flux coming into the heat sink, as it was used to determine the difference of thermal resistances between designs. In a real-life application with an IGBT [Fairchild Semiconductor

Corporation, 2008], the heat source would have a transient state behaviour of heat flux passing through the heat sink.

The temperature in a heat sink design will stay constant with time in a steady state heat flux, whereas the temperature in a heat sink design with transient behaviour heat flux will vary with time.

Simulations in transient state of heat flux were made for a design of a heat sink to determine if the varying temperature would exceed the threshold of a IGBT maximum operating conditions of 423 K.

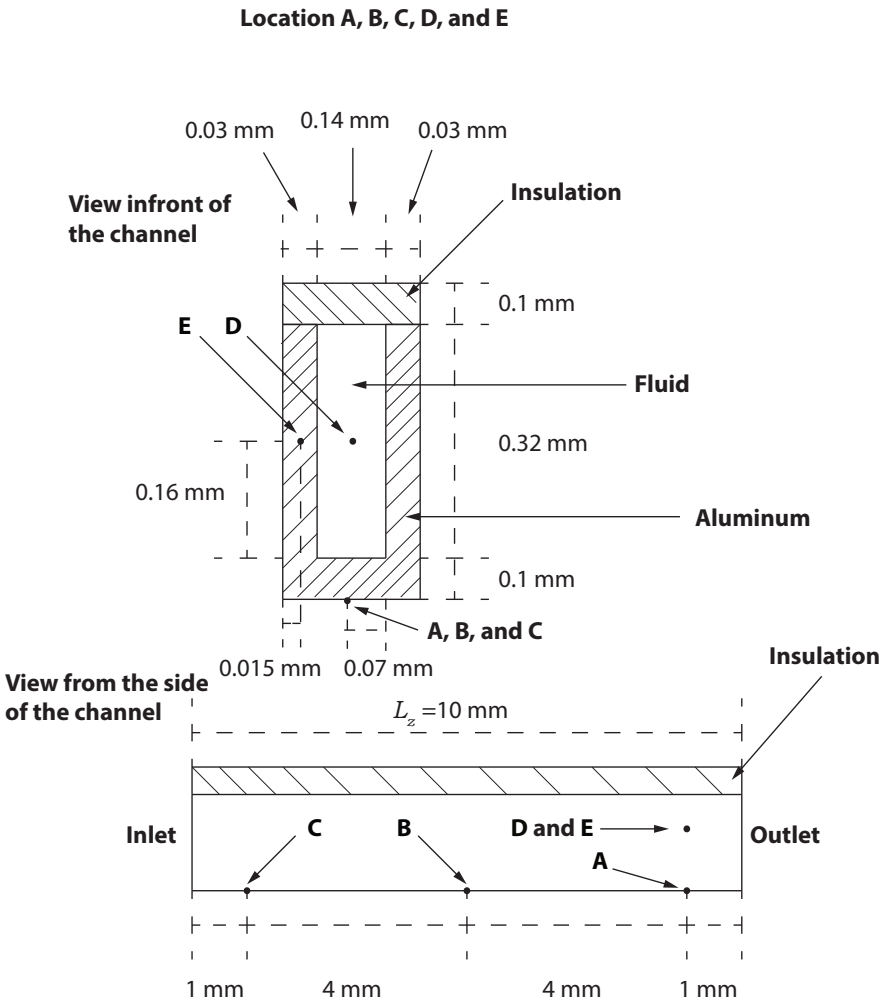

Figure 6.5: Locations of analysed temperature fluctuation

Figure 6.6 shows selected locations of **A**, **B**, **C**, **D**, and **E** in the optimal design of the heat sink with 50 channels and a β of 0.7, H = 0.32 mm, w_c=0.14, w_f=0.06 mm and w_p=0.2 mm.

Location **A** is at the base of the heat sink as T_{solid} in the calculations for optimum design in a steady state. The temperature fluctuation at location **A** was compared to the temperature fluctuation at locations **B** and **C** to see how specific locations along the length of the heat sink would be affected by the transient behavior of the heat flux at different pumping power ($\overline{P}$). Furthermore, location **A** was also compared to locations at the same cross-sectional area in the channel, 9 mm away from the inlet and 1 mm away from the outlet. With location **D** at the middle of the fluid flow and location **E** at the middle of fin in the channel. These locations were selected to see how transient heat flux effects different areas of the channel in terms of temperature.

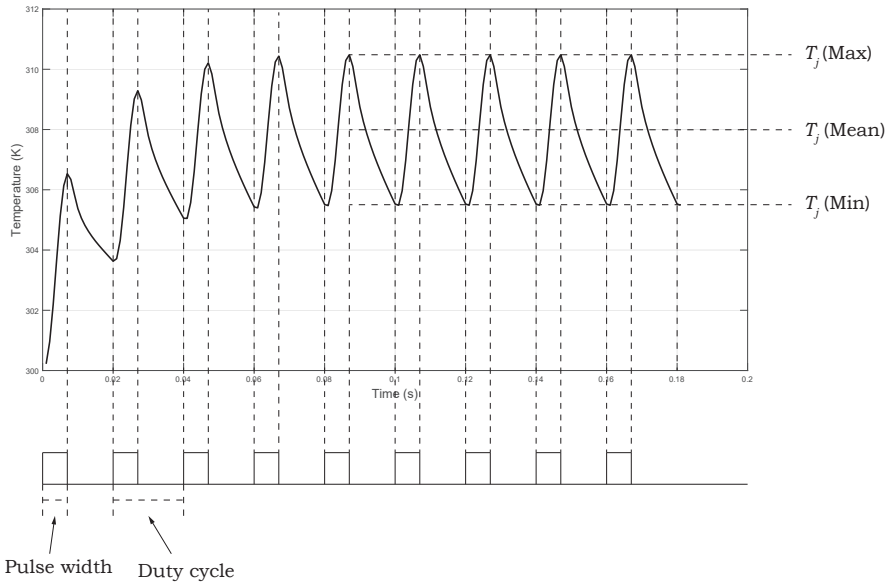

Figure 6.6: Parameters of junction temperature and frequency at location **A**

Location **A** exemplary illustrates how temperatures vary when a transient mean heat flux of 500 kW/m^2 is used at a $\overline{P}$ of 0.01 W in figure 6.6.

An IGBT [Fairchild Semiconductor Corporation, 2008] is assumed to be used for power electronics such as solar inverter application [Chou, 2008], whose output frequency fr is typically 50 Hz.

A frequency of 50 Hz means that there are fifty duty cycles per second in the simulation. The electronic device uses pulse mode as an operating system. The pulse mode has an on and off switch, where the heat is dissipated to the heat sink when the switch is on. One cycle of the electronic device being turned on and off is called a duty cycle [Tan et al., 2005].

T_j is the junction temperature, T_j(Max) indicates the peak temperature of 310.48 K in the simulation after the fluctuation of the temperature has stabilized. Subsequently, T_j(Mean) is the average temperature of 307.98 k and T_j(Min) is the minimum temperature of 305.49 of the junction temperature. Variation of the temperature stabilizes just before 0.1 s, after four duty cycles.

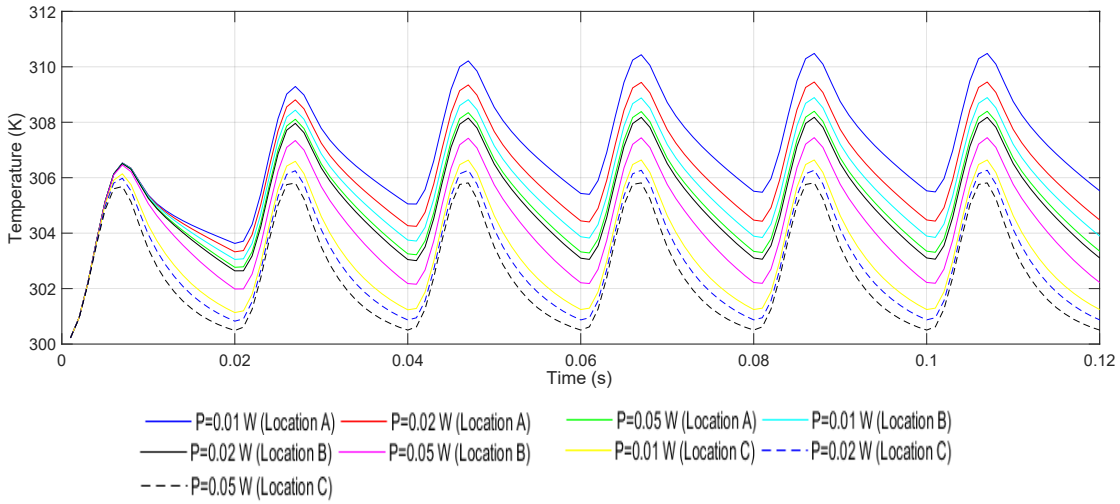

Figure 6.7: Fluctuating temperature at 50 Hz at location **A**, **B**, and **C** for a transient mean heat flux of 500 KW/m^2, with a $\overline{P}$ of 0.01, 0.02, and 0.05 W

Figure 6.7 shows the varying temperature at locations **A**, **B**, and **C** with a transient mean heat flux of 500 kW/m^2 at a frequency of 50 Hz. Pumping power was set at 0.01, 0.02 and 0.05 W to compare the junction temperature at different inlet velocities of 0.81, 1.15 and 1.82 m/s, respectively. The highest peak temperature T_j(Max) was 310.48 k at location **A** with a $\overline{P}$ of 0.01 W and the lowest temperature T_j(Min) is 300.62 K at location **C** with a $\overline{P}$ of 0.05 W.

The temperature fluctuation of T_j stabilizes at the same time for all designs in figure 6.7, after four duty cycles. This shows that the frequency is independent of the operating conditions in the simulation.

The largest range of temperature varying in T_j was at ΔT of 5.39 K for T_j(Max) of 307.45 K and T_j(Min) of 302.19 K at location **b** with a $\overline{P}$ of 0.05 W, where the T_j(Mean) is at 304.82 K.

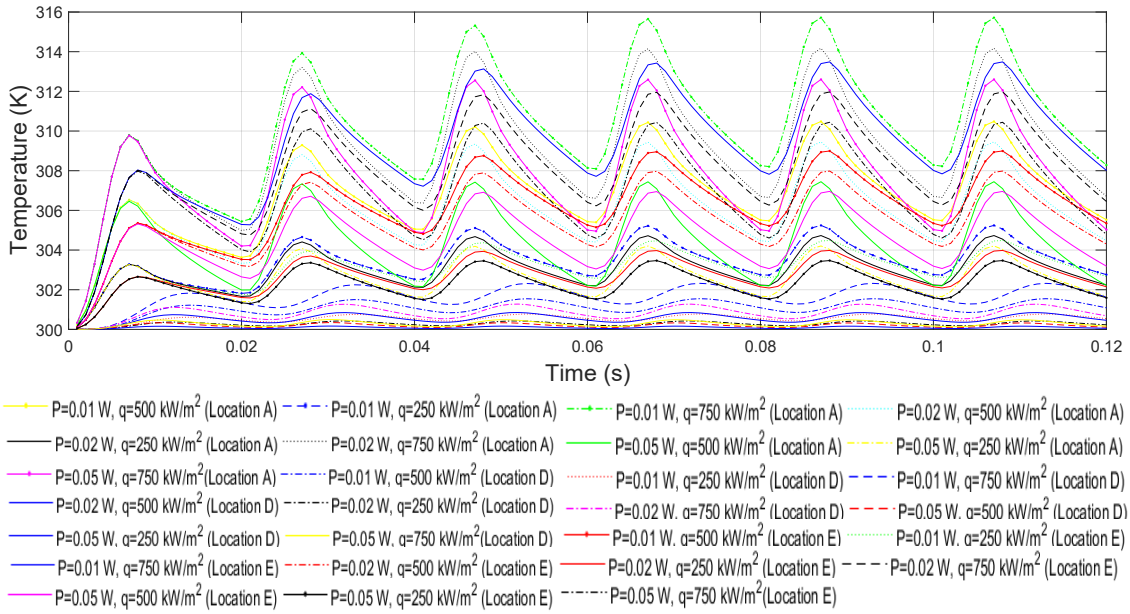

Figure 6.8: Varying temperature at 50 Hz for location **A**, **D**, and **E** at $\dot{q}_{mean}$ of 250 KW/m^2, 500 kW/m^2, and 750 KW/m^2, with a $\overline{P}$ of 0.01, 0.02, and 0.05 W

Figure 6.8 shows the varying temperature in a simulation at locations **A**, **D**, and **E** in the design. The operating conditions for this simulations were set at a $\overline{P}$ of 0.01, 0.02, and 0.05 W.

Additionally, the transient mean heat flux had different values of 500 kW/m^2, 250 kW/m^2, and 750 kW/m^2.

The highest peak temperature T_j(Max) was 315.72 k at location **A** with a pumping power of 0.01 W and mean heat flux of 750 kW/m^2. The lowest temperature T_j(Min) was 300.05 K at location **D** with a pumping power of 0.05 W and mean heat flux of 250 kW/m^2.

The largest range of temperature varying in T_j was ΔT of 7.63 K for T_j(Max) of 312.6 K and T_j(Min) of 304.97 K. This was at location **A** with a $\overline{P}$ of 0.05 W and a mean heat flux of 750 kW/m^2.

The location least effected by the changes in operating conditions in the simulation, was location **D** in the middle of the fluid medium in the design. Both location **A** and **E** are located at the solid medium in the design, which means that the fluid medium is less sensitive to changes in the operating conditions.

Furthermore, the highest temperature at a frequency of 50 Hz was at location **A** in previous simulations of 6.7 and 6.8. This showed that the temperature increased in correlation with increasing transient mean heat flux. By slowing down the frequency of the heat coming into the heat sink, would mean that they heat sink would be exposed higher heat flux for a longer period of time.

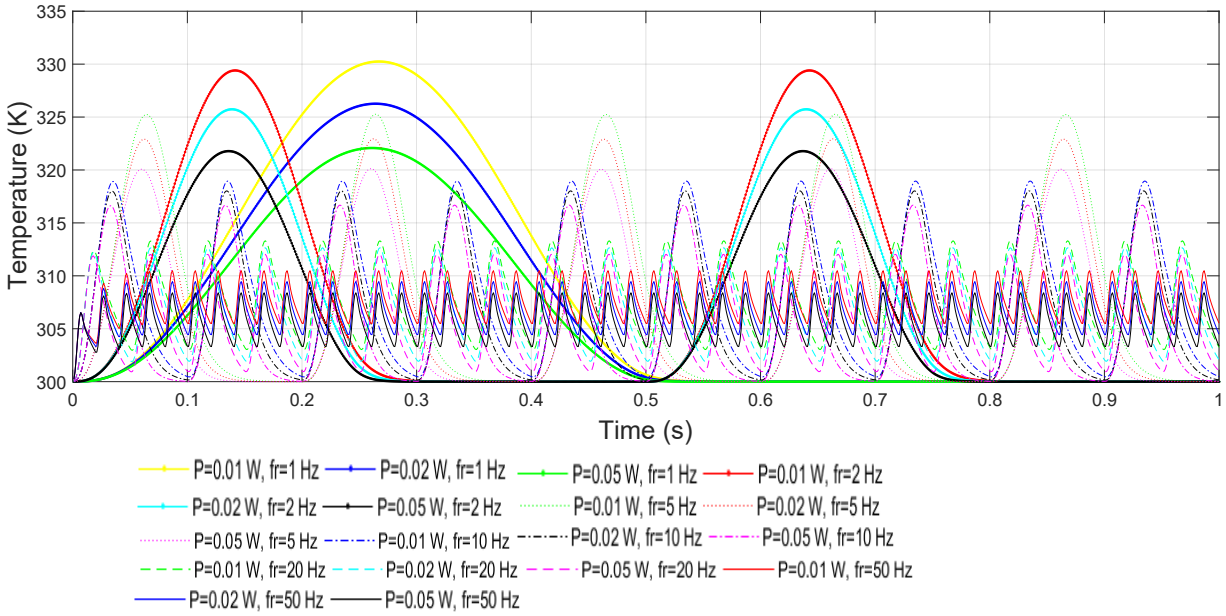

Figure 6.9: Varying temperature at a frequency of 1, 2, 5, 10, 20, and 50 Hz at location **A** for a heat flux of 500 KW/m^2 with the $\overline{P}$ of 0.01, 0.02, and 0.05 W

Figure 6.9 shows how the temperature rises at an increasing frequency in the simulations. The analysed time t interval was at 1 s, where simulation at a frequency of 1 Hz had one duty cycle in the interval. The number of duty cycles in the interval gets less as the frequency decreases.

The highest peak temperature T_j(Max) was 330.24 K at a frequency of 1 Hz and a $\overline{P}$ of 0.01 W. With a ΔT of 20 K from the highest temperature from frequency of 50 Hz. Which means that a lower frequency will reach a higher temperature in

the design.

The lowest temperature in the simulation for a frequency of 1 Hz was at 300 K, which is the initial temperature of the fluid. This is due to the longevity of the duty cycle. The temperature falls down to the initial temperature of the fluid at the end of the pulse width and remains there throughout the time interval of the duty cycle.

Frequencies of 2 and 5 Hz also fall down to the initial temperature of the fluid in the duty cycle. The results showed that a simulation of the design at a frequency of 10 Hz was the lowest frequency not to fall down to the initial fluid temperature, with the lowest temperature at 300.3 K.

Discussion

7

This chapter will discuss the method and result obtained from previous chapters in this study.

The study gave an overview of literature that was relative to the subject at hand in state of art, with an optimisation method from Li and Peterson [2006] used in this study to obtain the optimal design of a heat sink for a rectangular aluminum micro channel.

The optimization method by Li and Peterson [2006] has been utilised together with ANSYS Fluent CFD simulations for different designs of heat sinks in this study.

A design in the heat sink was compared to a theoretical velocity profile in a channel from White [1974] in CH.5.3.7, where the simulation in this study showed minimal marginal error compared to the velocity profile along the width and the height of the channel. However, the theoretical velocity profile has shown an slightly higher value at the center line in the channel than the numerical results from this study.

A 3D model of a channel of the heat sink has been modelled and meshed. Furthermore, with the required parameters and boundary conditions for its analysis by CFD methods, the system has been yield numerical results for different design configurations. Hence, three different channel geometries and heat flux values throughout the heat sink, have been simulated. Moreover, steady state and transient conditions for the specific heat sink application have been simulated.

A grid independence study has been done in CH. 5.3.7 to determine the minimum amount of nodal points needed without compromising the quality of the simulations. This grid study showed that, with the chosen grid of 787.500 cells, the results are inside the acceptable range from experimental results.

Validation of the usage of ANSYS in this study has been done by comparing simulated results of thermal resistance (R_t) to existing results from the experimental

study of Tuckerman and Pease [1981] and the numerical study of Toh et al. [2002] in CH. 5.3.8.

Table 7.1: Comparison of thermal resistance between experimental and computational results

Interface	Channel 1	Channel 2	Channel 3
R_t (K/W) [Tuckerman and Pease, 1981]	0.110	0.113	0.09
R_t (K/W) [Toh et al., 2002]	0.157	0.128	0.105
R_t (K/W) Current study	0.149	0.120	0.104

This comparison has shown that the results obtained are inside the experimental values of the bibliography.

Results of all the designs specified in CH. 5.1.1 were displayed in CH. 6.1, where the micro channel heat sink with the lowest R_t was at 80 channels with β of 0.8. From an engineering point of view that was the optimal design of the heat sink, however, taking into consideration the cost of making a customized heat sink, the optimal design of heat sink was considered to be N of 50 with β 0.7 in CH. 6.2. The following figures show the temperature distribution of the optimal case in the channel and the base of the heat sink.

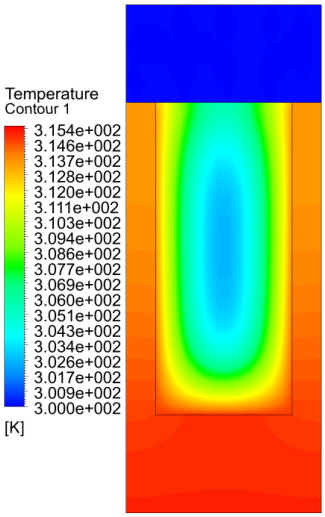

Figure 7.1: Temperature contour at cross-sectional area at 9 mm away from the inlet at the at the optimal design

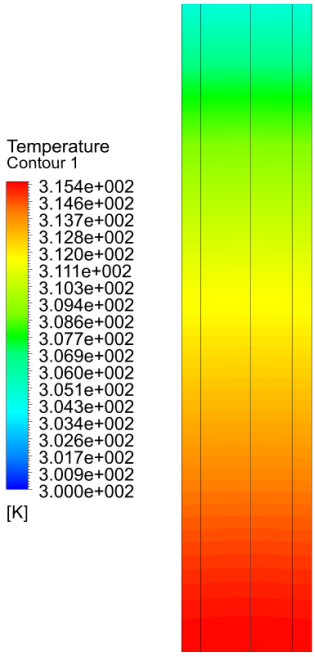

Figure 7.2: Temperature contour at the base of the optimal design of the heat sink

Simulations at a transient behavior for a mean heat flux coming into the heat sink at a constant $\overline{P}$ were conducted for the chosen optimal design in CH. 6.4. This transient analysis was focused on the fluctuation of temperature at five different locations in the design, at different operating conditions. It was shown that the locations at the solid area in the design are more sensitive to changes in the operating conditions of $\overline{P}$ and transient mean heat flux, then the location in the fluid.

The value of temperature increases with a lower frequency. As an example, in the heat sink base, a peak temperature at a frequency of 50 Hz is 310.5 K whereas the peak temperature for 1 Hz is 330 K.

Conclusion

8

This chapter presents this study's key results and summarises the project's findings.

This study has introduced the theoretical background and methodology to effectively model a heat dissipation procedure for an IGBT with the use of a forced convection with a liquid in a micro channel heat sink. Furthermore, the software Ansys fluent has been used to generate solutions for different geometries and working configurations.

Heat transfer in fluid media is governed by the Fourier and Navier-Stokes equation that describes both solid and fluid interactions of momentum and energy.

Typical heat dissipation devices (like a heat sink) use the interaction between fluid and solid media and try to maximize the contact area between both. This maximisation of contact area is done by the use of fins. Hence, heat transfer is highly influenced by the efficient use of fins as well as the properties of both media, the fluid momentum, and surrounding temperatures. Moreover, for a micro channel heat sink the height, width and the number of channels define the contact area between both media.

For the optimal heat sink design found in this study (considering heat flux, pumping power, frequency, number of channels, height of fin, width of fin, and temperature at the inlet), it has been shown that theoretical and experimental results correlate with the result obtained in this study with only marginal error. The temperature distribution for the heat sink showed a maximum temperature of the IGBT of 330 K. This is considered a good result taking into consideration that that IGBT [Fairchild Semiconductor Corporation, 2008] has a maximum operating temperature of 423 K; working at 26 % of its maximum thermal capability.

Results obtained from this have been compared with experimental and numerical results from Tuckerman and Pease [1981] and Toh et al. [2002]. This comparison

has shown that the results obtained have a mean error of 19 % and 4 %, respectively. Although the results of Toh et al. [2002] correspond more accurately with this thesis' results, the experimental result of [Tuckerman and Pease, 1981] indicate that an improvement in the CFD simulations can be achieved in future work. Nevertheless, the results in this study show physical logic and no major disparities are shown. Regarding the improvement of the model, a greater use of resources in terms of computational power and grid size, could greatly enhance the results obtained by it.

Furthermore, the analysis showed that the thermal resistance decreases with an increasing number of channels in the heat sink designs. However, at one point, the analyzed heat sinks' purchasing cost rise disproportionally to their thermal performance. The optimal micro channel heat sink design in regards to both thermal dissipation and purchasing cost was identified to have 50 channels and a 0.7 width ratio between fins and channels.

Future Work

9

This chapter presents the topics and analyses that this thesis has not addressed and could be interesting and relevant to study further.

This thesis can be used as a base for simulating with CFD for a micro channel heat sink in both steady state and transient conditions. However, it would be desirable to fulfill the following tasks in future research:

- Experimental study: The purchase of the simulated heat sink and its evaluation in a lab for comparison and validation purposes would be desirable.
- Enhance CFD simulation: A more refined mesh with a special effort placed in the boundary layer and the interfaces; and the simulation of the whole heat sink and not only a channel would generate more accurate solution. Furthermore, the integration turbulence modelling, higher flow velocities, and/or Large Eddy Simulation/Direct Numerical Simulation (ELS/DNS), if the available computational power allows it would be highly accurate

Bibliography

Ahmed et al., **2018**. Hamdi E Ahmed, BH Salman, A Sh Kherbeet and MI Ahmed. *Optimization of thermal design of heat sinks: A review.* International Journal of Heat and Mass Transfer, 118, 129–153, 2018.

Anderson and Wendt, **1995**. John David Anderson and J Wendt. *Computational fluid dynamics*, volume 206. Springer, 1995.

Arora, **2004**. Jasbir Singh Arora. *Introduction to optimum design.* Elsevier, 2004.

Bello-Ochende et al., **2007**. T Bello-Ochende, L Liebenberg and JP Meyer. *Constructal design: geometric optimization of micro-channel heat sinks.* South African Journal of Science, 103(11-12), 483–489, 2007.

Bergman et al., **2011**. Theodore L Bergman, Frank P Incropera, Adrienne S Lavine and David P DeWitt. *Introduction to heat transfer.* John Wiley & Sons, 2011.

Bhaskaran and Collins, **2002**. Rajesh Bhaskaran and Lance Collins. *Introduction to CFD basics.* Cornell University-Sibley School of Mechanical and Aerospace Engineering, page 32, 2002.

Celik et al., **2008**. Ishmail B Celik, Urmila Ghia, Patrick J Roache et al. *Procedure for estimation and reporting of uncertainty due to discretization in {CFD} applications.* Journal of fluids {Engineering-Transactions} of the {ASME}, 130 (7), 2008.

Cengel, **2010**. Yunus A Cengel. *Fluid mechanics.* Tata McGraw-Hill Education, 2010.

Chazelle and Edelsbrunner, **1992**. Bernard Chazelle and Herbert Edelsbrunner. *An optimal algorithm for intersecting line segments in the plane.* Journal of the ACM (JACM), 39(1), 1–54, 1992.

Chen and Chen, **2013**. Chyi-Tsong Chen and Hung-I Chen. *Multi-objective optimization design of plate-fin heat sinks using a direction-based genetic algorithm.* Journal of the Taiwan Institute of chemical Engineers, 44(2), 257–265, 2013.

Chingulpitak et al., **2016**. Sakkarin Chingulpitak, Nares Chimres, Kitti Nilpueng and Somchai Wongwises. *Experimental and numerical investigations of heat transfer and flow characteristics of cross-cut heat sinks*. International Journal of Heat and Mass Transfer, 102, 142–153, 2016.

Chou, **2008**. Wibawa Chou. *Choose your IGBTs correctly for solar inverter applications*. Power Electronics, 2008.

Dou, **2005**. Hua-Shu Dou. *Energy gradient theory of hydrodynamic instability*. arXiv preprint nlin/0501049, 2005.

elements. American elements. *Silicon wafer, year = 1998, url = https://www.americanelements.com/silicon-wafer-7440-21-3, urldate = 2019-03-17*.

Ermagan and Rafee, **2018**. Hamidreza Ermagan and Roohollah Rafee. *Geometric optimization of an enhanced microchannel heat sink with superhydrophobic walls*. Applied Thermal Engineering, 130, 384–394, 2018.

Euromoney Institutional Investor PLC, **2019**. Euromoney Institutional Investor PLC. *LME base metal prices and charts*, 2019. URL `https://www.fastmarkets.com/commodities/exchange-data/lme-base-metal-prices-and-charts`.

Fairchild Semiconductor Corporation, **2008**. Fairchild Semiconductor Corporation. *FGH40N60UFD*, 2008. URL `https://www.promelec.ru/pdf/FGH40N60UFD.pdf`. original document from Fairchild.

Ferrás et al., **2012**. LL Ferrás, AM Afonso, MA Alves, JM Nóbrega and FT Pinho. *Development length in planar channel flows of Newtonian fluids under the influence of wall slip*. Journal of Fluids Engineering, 134(10), 104503, 2012.

Gerhart et al., **2016**. Philip M Gerhart, Andrew L Gerhart and John I Hochstein. *Munson, Young and Okiishi's Fundamentals of Fluid Mechanics, Binder Ready Version*. John Wiley & Sons, 2016.

Hamburgen, **1986**. William R Hamburgen. *Optimal finned heat sinks*. Digital Equipment Corporation Western Research Laboratory [WRL], 1986.

Hanks and Ruo, **1966**. Richard W Hanks and H-C Ruo. *Laminar-turbulent transition in ducts of rectangular cross section*. Industrial & Engineering Chemistry Fundamentals, 5(4), 558–561, 1966.

Hazarika et al., **2016**. Saheera Azmi Hazarika, Dipankar Bhanja, Sujit Nath and Balaram Kundu. *Geometric optimization and performance study of a constructal T-shaped fin under simultaneous heat and mass transfer*. Applied Thermal Engineering, 109, 162 – 174, 2016. ISSN 1359-4311. doi: https://doi.org/10.1016/j.applthermaleng.2016.08.007. URL `http://www.sciencedirect.com/science/article/pii/S1359431116313539`.

Husain and Kim, **2008**. Afzal Husain and Kwang-Yong Kim. *Shape optimization of micro-channel heat sink for micro-electronic cooling*. IEEE Transactions on Components and Packaging Technologies, 31(2), 322–330, 2008.

Karathanassis et al., **2013**. Ioannis K Karathanassis, Elias Papanicolaou, Vassilios Belessiotis and Georgios C Bergeles. *Multi-objective design optimization of a micro heat sink for Concentrating Photovoltaic/Thermal (CPVT) systems using a genetic algorithm*. Applied Thermal Engineering, 59(1-2), 733–744, 2013.

Takahiro Katoh, Guoping Xu, Marlin Vogel and Shlomo Novotny, *2004*. Takahiro Katoh, Guoping Xu, Marlin Vogel and Shlomo Novotny. New attempt of forced-air cooling for high heat-flux applications. In *The Ninth Intersociety Conference on Thermal and Thermomechanical Phenomena In Electronic Systems (IEEE Cat. No. 04CH37543)*, volume 2, pages 34–39. IEEE, 2004.

Kays, **2012**. William Morrow Kays. *Convective heat and mass transfer*. Tata McGraw-Hill Education, 2012.

Kays and Crawford, **1993**. William Morrow Kays and Michael E Crawford. *Convective heat and mass transfer*. BOOK. McGraw-Hill, 1993.

Kiijarvi, **2011**. Jukka Kiijarvi. *Darcy friction factor formulae in turbulent pipe flow*. Lunowa Fluid Mechanics Paper, 110727, 1–11, 2011.

Kim, **2014**. Dong-Kwon Kim. *Thermal optimization of branched-fin heat sinks subject to a parallel flow*. International Journal of Heat and Mass Transfer, 77, 278 – 287, 2014. ISSN 0017-9310. doi: https://doi.org/10.1016/j.ijheatmasstransfer.2014.05.010. URL `http://www.sciencedirect.com/science/article/pii/S0017931014004104`.

Knight et al., **1992a**. Roy W Knight, Donald J Hall, John S Goodling and Richard C Jaeger. *Heat sink optimization with application to microchannels*. IEEE Transactions on Components, Hybrids, and Manufacturing Technology, 15(5), 832–842, 1992.

Knight et al., **1992b**. R.W. Knight, J.S. Goodling and B.E. Gross. *Optimal thermal design of air cooled forced convection finned heat sinks-experimental verification.* IEEE Transactions on Components, Hybrids, and Manufacturing Technology, 15(5), 754–760, 1992.

Kreith et al., **2012**. Frank Kreith, Raj M Manglik and Mark S Bohn. *Principles of heat transfer.* Cengage learning, 2012.

Kudela, **2010**. Henryk Kudela. *Hydraulic losses in pipes.* Chart, (3), 9, 2010.

Lee, **1995**. Seri Lee. *Optimum design and selection of heat sinks.* IEEE Transactions on Components, Packaging, and Manufacturing Technology: Part A, 18(4), 812–817, 1995.

Li and Peterson, **2007**. J. Li and G.P. Peterson. *3-Dimensional numerical optimization of silicon-based high performance parallel microchannel heat sink with liquid flow.* International Journal of Heat and Mass Transfer, 50(15), 2895 – 2904, 2007. ISSN 0017-9310. doi: https://doi.org/10.1016/j.ijheatmasstransfer.2007.01.019. URL `http://www.sciencedirect.com/science/article/pii/S0017931007000865`.

Li and Peterson, **2006**. Ji Li and GP Peterson. *Geometric optimization of a micro heat sink with liquid flow.* IEEE Transactions on Components and Packaging Technologies, 29(1), 145–154, 2006.

Lombard, **2008**. Matt Lombard. *SolidWorks 2007 Bible*, volume 529. John Wiley & Sons, 2008.

Lorenzini et al., **2011**. Giulio Lorenzini, Simone Moretti and Alessandra Conti. *Fin shape thermal optimization using Bejan's constructal theory.* Synthesis Lectures on Engineering, 6(1), 1–219, 2011.

Majumdar, **2005**. Pradip Majumdar. *Computational methods for heat and mass transfer.* CRC press, 2005.

K Marzec and A Kucaba-Pietal, *2014*. K Marzec and A Kucaba-Pietal. Heat transfer characteristic of an impingement cooling system with different nozzle geometry. In *Journal of Physics: Conference Series*, volume 530, page 012038. IOP Publishing, 2014.

Micro Logic Corporation, **2004**. Micro Logic Corporation. *emachineshop*, 2004. URL `https://www.emachineshop.com/`.

Mills, **1992**. Anthony F Mills. *Heat transfer*, volume 1. Burr Ridge, Ill. : Irwin, 1992.

Peles et al., **2005**. Yoav Peles, Ali KoÅŸar, Chandan Mishra, Chih-Jung Kuo and Brandon Schneider. *Forced convective heat transfer across a pin fin micro heat sink*. International Journal of Heat and Mass Transfer, 48(17), 3615 – 3627, 2005. ISSN 0017-9310. doi: https://doi.org/10.1016/j.ijheatmasstransfer.2005.03.017. URL `http://www.sciencedirect.com/science/article/pii/S0017931005002255`.

Powell et al., **1966**. RW Powell, Cho Yen Ho and Peter Edward Liley. *Thermal conductivity of selected materials*, volume 8. US Government Printing Office Washington, D. C, 1966.

Prabhakara and Deshpande, **2004**. Sandeep Prabhakara and MD Deshpande. *The no-slip boundary condition in fluid mechanics*. Resonance, 9(5), 61–71, 2004.

Roache, **1998**. P J Roache. *Verification and validation in computational science and engineering*. Hermosa, Albuquerque, NM, 1998. URL `http://cds.cern.ch/record/580994`.

Roache et al., **1986**. Patrick J Roache, Kirti N Ghia and Frank M White. *Editorial policy statement on the control of numerical accuracy*. Journal of Fluids Engineering, 108(1), 2–2, 1986.

Peter Rodgers and Valérie Eveloy, *2013*. Peter Rodgers and Valérie Eveloy. Air cooled heat sink design optimization in free convection. In *29th IEEE Semiconductor Thermal Measurement and Management Symposium*, pages 170–172. IEEE, 2013.

Rybiński and Mikielewicz, **2014**. Witold Rybiński and Jarosław Mikielewicz. *Analytical solutions of heat transfer for laminar flow in rectangular channels*. Archives of Thermodynamics, 35(4), 29–42, 2014.

Manish Saini and Ralph L Webb, *2002*. Manish Saini and Ralph L Webb. Heat rejection limits of air cooled plane fin heat sinks for computer cooling. In *Thermal and Thermomechanical Phenomena in Electronic Systems, 2002. ITHERM 2002. The Eighth Intersociety Conference on*, pages 1–8. IEEE, 2002.

Sasaki and Kishimoto, **1986**. S. Sasaki and T. Kishimoto. *OPTIMAL STRUCTURE FOR MICROGROOVED COOLING FIN FOR HIGH-POWER LSI DEVICES*. Electronics Letters, 22(24), 1332–1334, 1986.

Shafiee and Topal, **2009**. Shahriar Shafiee and Erkan Topal. *When will fossil fuel reserves be diminished?* Energy policy, 37(1), 181–189, 2009.

Smith et al., **October 14 2014**. Charles Gordon Smith, Richard L Knipe, Vikram Joshi, Roberto Gaddi, Anartz Unamuno and Robertus Petrus Van Kampen. *Device containing plurality of smaller MEMS devices in place of a larger MEMS device*, 2014. US Patent 8,861,218.

Stolarski et al., **2018**. Tadeusz Stolarski, Yuji Nakasone and Shigeka Yoshimoto. *Engineering analysis with ANSYS software*. Butterworth-Heinemann, 2018.

Sui et al., **2010**. Y Sui, CJ Teo, Poh Seng Lee, YT Chew and C Shu. *Fluid flow and heat transfer in wavy microchannels*. International Journal of Heat and Mass Transfer, 53(13-14), 2760–2772, 2010.

Tan et al., **2005**. Siew-Chong Tan, YM Lai and Chi K Tse. *Implementation of pulse-width-modulation based sliding mode controller for boost converters*. IEEE Power Electronics Letters, 3(4), 130–135, 2005.

Toh et al., **2002**. KC Toh, XY Chen and JC Chai. *Numerical computation of fluid flow and heat transfer in microchannels*. International Journal of Heat and Mass Transfer, 45(26), 5133–5141, 2002.

Treadgold, **December 2018**. Tim Treadgold. *Shrinking Stockpiles Put Copper On Track For A Price Rise Despite Trade War Uncertainty*, 2018. URL `https://www.forbes.com/sites/timtreadgold/2018/12/11/shrinking-stockpiles-put-copper-on-track-for-a-price-rise-despite-trade-war-uncerta#2e8921a688bc`. [Online; posted 11-December-2018].

Tuckerman and Pease, **1981**. David B Tuckerman and Roger Fabian W Pease. *High-performance heat sinking for VLSI*. IEEE Electron device letters, 2(5), 126–129, 1981.

United Nations Department of Economic and Social Affairs, **2017**. United Nations Department of Economic and Social Affairs. *World Population Prospects - The 2017 Revision*. World Population Prospects The 2017, pages 1–46, 2017. URL `https://esa.un.org/unpd/wpp/Publications/Files/WPP2017{_}KeyFindings.pdf`.

Versteeg and Malalasekera, **2007**. Henk Kaarle Versteeg and Weeratunge Malalasekera. *An introduction to computational fluid dynamics: the finite volume method*. Pearson education, 2007.

WELSH, **1954**. JAMES P WELSH. *A Guide Manual of Cooling Methods for Electronic Equipment*, CORNELL AERONAUTICAL LAB INC BUFFALO NY, 1954.

Welty et al., **2009**. James R Welty, Charles E Wicks, Gregory Rorrer and Robert E Wilson. *Fundamentals of momentum, heat, and mass transfer*. John Wiley & Sons, 2009.

White, **1974**. Frank M White. *Solutions Manual to Accompany Viscous Fluid Flow*. McGraw-Hill, 1974.

Whitfield, **2008**. Stephen J Whitfield. *A Companion to 20th-century America*. John Wiley & Sons, 2008.

Xianghui and Feng, **2011**. SU Xianghui and XU Feng. *Transient Thermal Analysis of a Plate Fin Heat Sink with Green's Function*. Chinese Journal of Aeronautics, 24(3), 243–248, 2011.

Zeng et al., **2018**. Shi Zeng, Bugra Kanargi and Poh Seng Lee. *Experimental and numerical investigation of a mini channel forced air heat sink designed by topology optimization*. International Journal of Heat and Mass Transfer, 121, 663–679, 2018.

Zhao and Lu, **2002**. CY Zhao and TJ Lu. *Analysis of microchannel heat sinks for electronics cooling*. International Journal of Heat and Mass Transfer, 45(24), 4857–4869, 2002.

Zheng and Silber-Li, **2008**. Xu Zheng and Zhan-hua Silber-Li. *Measurement of velocity profiles in a rectangular microchannel with aspect ratio $\alpha = 0.35$*. Experiments in Fluids, 44(6), 951–959, 2008.

Zhou et al., **2016**. Jiandong Zhou, M Hatami, Dongxing Song and Dengwei Jing. *Design of microchannel heat sink with wavy channel and its time-efficient optimization with combined RSM and FVM methods*. International Journal of Heat and Mass Transfer, 103, 715–724, 2016.

Çengel, **2011**. Yunus A. Çengel. *Fundamentals of Heat and Mass Transfer*. McGraw Hill, 3^{th} edition, 2011. ISBN 978-0071257398.

Appendix A

Grid independency background theory

In a article from Celik et al. [2008] the recommended steps taken in solving the estimation of the discretization error are featured.

For the calculation of three dimensional simulations, the grid size h is acquired by using following equation,

$$h = \left[\frac{1}{N} \sum_{i=1}^{N} (\Delta V_i) \right]^{1/3} \tag{A.1}$$

where ΔV_i is the volume and N is the total number of cells. The difference between exact and discrete solution can be defined as solution error, the solution error is involved in the apparent order P of the grid convergence

$$p = \frac{1}{ln(r_{21})} \left| ln \left| \varepsilon_{32}/\varepsilon_{21} \right| + q(p) \right| \tag{A.2}$$

$$q(p) = ln \left(\frac{r_{21}^{p} - s}{r_{32}^{p} - s} \right) \tag{A.3}$$

$$s = 1 \cdot sgn \left(\varepsilon_{32}/\varepsilon_{21} \right) \tag{A.4}$$

where $\varepsilon_{ij} = \phi_{coarse} - \phi_{fine}$ is the ratio between selected values ϕ, such as pressure loss or velocity from different grid sizes. The ratio between the values of the grid sizes can not be very close to zero or the procedure will not work. The same goes for a negative results, which are a indication of oscillatory convergence.

The extrapolated values ϕ_{ext} are values that are estimated of a variables by using extrapolation. If a variable is beyond the range of initial observation, the extrapolation uses connection of variable beyond the initial observation range with a variable inside the initial observation range to estimate the value of the variable.

$$\phi_{ext}^{21} = \left(r_{21}^{p}\phi_1 - \phi_2\right) / \left(r_{21}^{p} - 1\right) \tag{A.5}$$

To find the ratio between approximate error and the present approximation, the approximate relative error e_a^{21} is used.

$$e_a^{21} = \left|\frac{\phi_1 - \phi_2}{\phi_1}\right| \tag{A.6}$$

Extrapolated relative error e_{ext}^{21} can be found by using the following equation,

$$e_{ext}^{21} = \left|\frac{\phi_{ext}^{21} - \phi_1}{\phi_{ext}^{21}}\right| \tag{A.7}$$

The fine-grid convergence index GCI_{fine}^{21} is the percentage of how far computed value is distanced from the asymptotic numerical value.

$$GCI_{fine}^{21} = \frac{1.25e_a^{21}}{r_{21}^{p} - 1} \tag{A.8}$$

A range of error (*error band*) is set on both sides of the GCI_{fine}^{21}, as the true value of the solution is thought to be inside the error band.

$$\phi_{range} = \phi_{ext} \pm \phi_{ext} \cdot GCI_{fine}^{21} \tag{A.9}$$

If all grid sizes are within the error band, then the size with the least amount of grids is the most suitable to use [Celik et al., 2008].